INVESTIGATING THE EFFECTS OF ROOF DIAPHRAGM STIFFNESS ON THE FORCE TRANSFERRED AT THE WALL AND DIAPHRAGM INTERFACE IN LOW-RISE MASONRY CONSTRUCTION

By

NEIL BENNETT MANGOLD

A thesis submitted in partial fulfillment of
the requirements for the degree of

MASTER OF SCIENCE IN CIVIL ENGINEERING

WASHINGTON STATE UNIVERSITY
Department of Civil and Environmental Engineering

MAY 2014

To the Faculty of Washington State University:

The members of the Committee appointed to examine the thesis of NEIL BENNETT MANGOLD find it satisfactory and recommend that it be accepted.

_____

J. Daniel Dolan, Ph.D., Chair

_____

William Cofer, Ph.D.

_____

Anthony Battistini, Ph.D.

Acknowledgements

Many people have contributed to the successful completion of this project. Many thanks to my Committee: Dr. Dan Dolan Dr. William Cofer, and Dr. Anthony Battistini, all of whom provided advice and guidance during times of frustration.

My special thanks are extended to my parents and aunt who provided encouragement and support throughout my entire graduate career. Most importantly, my sincerest gratitude is given to my wife Jennisa Mangold, without whom I would not have been successful.

INVESTIGATING THE EFFECTS OF ROOF DIAPHRAGM STIFFNESS ON THE FORCE TRANSFERRED AT THE WALL AND DIAPHRAGM INTERFACE IN LOW-RISE MASONRY CONSTRUCTION

Abstract

by Neil Bennett Mangold M.S.
Washington State University
May 2014

Chair: J. Daniel Dolan

The aim of this thesis is to investigate the effects of diaphragm stiffness on the force transferred at the wall/diaphragm interface in low-rise masonry structures. This type of construction is very typical in America, and in the past has been shown to be susceptible to out-of-plane wall and connection failures during seismic events. In order to prevent out of plane collapse of masonry walls, building code provisions require designers to directly connect walls on the opposing sides of a structure. This connection is created with a continuous structural member across the length of a building. This solution does not directly address the issue of failure at the wall/diaphragm interface.

In order to gain a better understanding of the forces transferred between the wall and diaphragm, this study developed finite element models to investigate this construction type. This investigation used a parametric study that covered a range of roof diaphragm properties and building aspect ratios that are common in practical construction. The results of the parametric study were used to draw conclusions about the effect of diaphragm stiffness on the magnitude of wall/diaphragm interaction forces and their distribution.

It was concluded that for a range of typical roof diaphragm properties, the force transferred by the walls into the diaphragm is relatively unaffected. For all building aspect ratios tested, the force in the connections at the wall/diaphragm interface exceeded the requirement of current design standards. This study serves as an initial investigation into the issues around the diaphragm/wall interface forces and provides groundwork for further research.

Table of Contents

List of tables

List of figures

1.0 Introduction

This chapter develops a basic foundation for understanding the questions addressed in this thesis. First, a background regarding the necessity for the research is provided. The scope of work is presented, as well as the primary goal of this thesis, and an outline of the following chapters.

1.1 Need for research

Many low-rise buildings are typically constructed of timber or metal deck roofs on masonry or concrete walls. This practice is most prevalent in the "big box" store style of construction. The focus of this paper is the seismic design/performance of this type of construction, and in particular, the forces developed in the connection between the diaphragm and the wall. Throughout this paper, the terms diaphragm and roof are synonymous and refer to metal or wood sheathed diaphragms. The term wall always means reinforced concrete or masonry wall construction. The type of roof considered is light and relatively flexible when compared to the concrete/masonry walls. The walls are typically between 15' and 40' tall with few openings. Flexible diaphragms connected to heavy and stiff walls result in the load path changing from the traditional simple beam analysis for the diaphragm to a beam on elastic foundation response. A labeled schematic of the building type being considered and an example of the building type being considered and the deflected shape under seismic load are presented in Figure 1.1 and Figure 1.2.

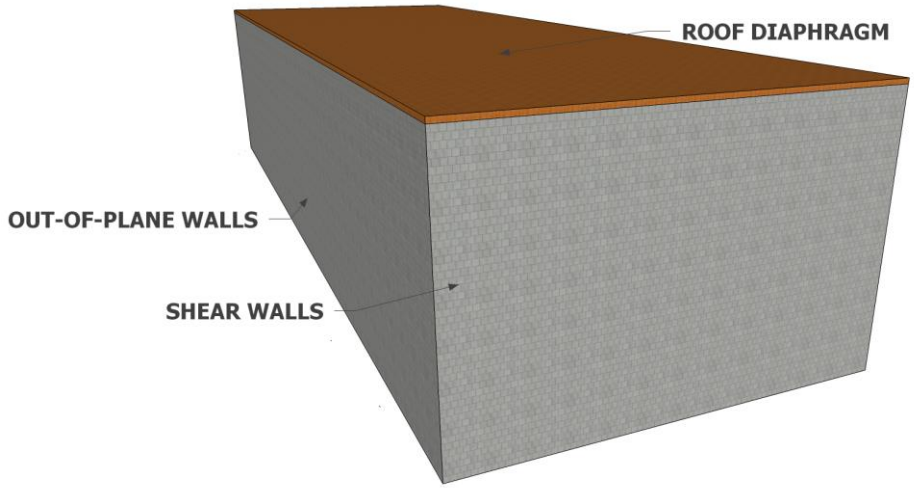

Figure 1.1 Typical Low-Rise Masonry Building

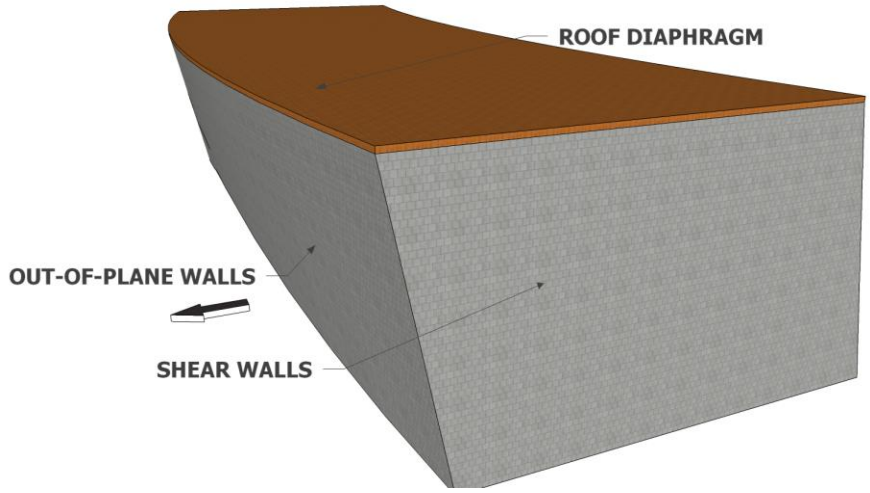

Figure 1.2 Deflected Low-Rise Masonry Building

Out of plane failures observed in the 1971 San Fernando and 1994 Northridge earthquakes have caused the close examination of anchorage forces between diaphragms and masonry walls. During these events many failures were observed to be caused by the high mass of the walls that could not be supported by the relatively light diaphragms. The results of these failures were the out-of-plane collapse

of the walls. An example of this type of failure in presented in Figure 1.3. In response to these failures, the International Building Code (IBC) (IBC § 1615.4.2.2) and the American Society of Civil Engineers (ASCE) (ASCE 7-10 §12.11.2.2.3 & §12.11.2.2.4) adopted changes to require sufficient strength to transfer the anchorage forces. For a more detailed discussion of this issue refer to "Anchorage of Concrete Walls" published in the winter 2005 issue of *Masonry Chronicles* (Ekwueme 2005).

Figure 1.3 Out-of-Plane Wall Failure Example

Continuous lateral ties are now required by the IBC to prevent the failure of anchorage connections. These ties work in two ways: by developing the anchorage forces deep into the diaphragm and by allowing parallel walls to push and pull on one another. During a seismic event, the connection activates the entire diaphragm and opposing wall instead of just a localized area at the diaphragm chord member. By moving the force away from the vulnerable connection, failures at the wall/diaphragm interface should be reduced. However this solution does not directly address the cause of failure, which

is located at the anchorage connection. An illustration of how these continuous lateral ties are positioned in a building is shown in Figure 1.4.

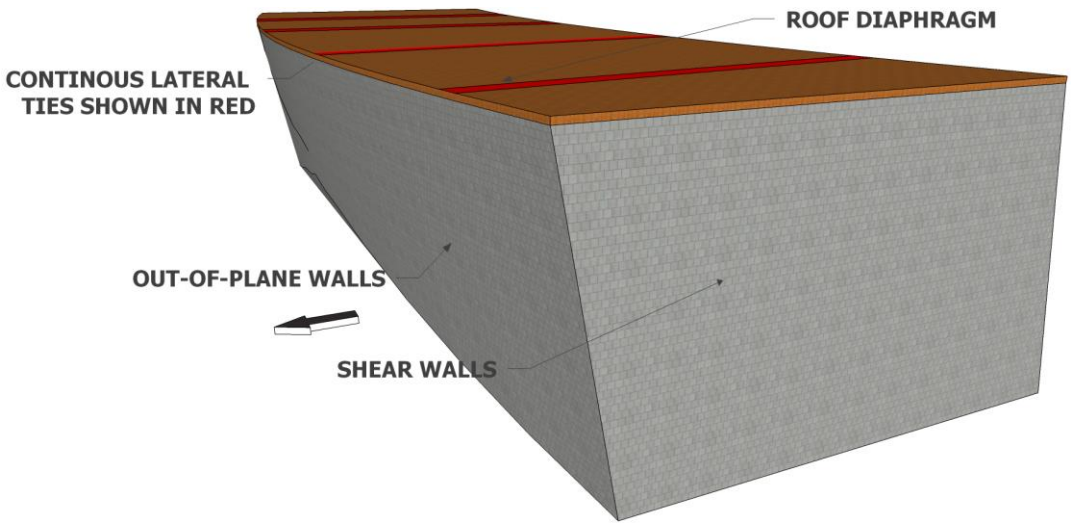

Figure 1.4 Illustration of Continuous Lateral Ties

Out of plane wall failure is due to the stiffness incompatibility of masonry and concrete walls with flexible diaphragms. Seismic forces are generated by inertial mass. Walls and diaphragms have significantly different masses, and therefore different responses. The relative stiffness of each element requires that the roof deflect much more than the wall before resisting equivalent loads. This means that the connection between these elements experiences very high stress due to the differences in deflections.

Historically, there has been little investigation into the effect of diaphragm stiffness on the connection at the wall/diaphragm interface. This is partly due to the lack of funding from the material industries because of the different in construction materials used for the roof and walls. Previous research has recognized the common failure at this connection. No study on the effects of the diaphragm flexibility on the wall/diaphragm connection has yet been completed.

1.2 Objective

The goal of this thesis is to report the results of a numerical study of the impact of diaphragm flexibility on the connection forces at the wall/roof interface. This study will improve the ability of the designer to consider the effects of the incompatibility of various structural elements. Results of this research will hopefully lead to better design practices and safer buildings.

1.3 Scope of work

In order to complete this study, finite element models were developed to examine the effects of diaphragm stiffness in low-rise masonry buildings. No physical testing was conducted, although data from wall, diaphragm, and bolt shear tests conducted by other researchers was used to validate models. All finite element models were developed using SAP2000 software. Each model was designed to analyze unidirectional loading only, and all elements were calibrated to respond to the particular loading direction. The models were tested under a series of configurations that varied the aspect ratio and diaphragm stiffness properties. Reported data consisted of the force transferred through the wall/diaphragm connection for each test.

2.0 Literature review

This literature review attempts to provide a background of the research that has already been applied to this topic. It starts with the discussion of the seismic response of low-rise construction, as this is the issue considered. Then an overview of research into flexible diaphragms and wall-diaphragm connections is provided.

2.1 Seismic response of low rise masonry buildings

Many studies have been conducted on the seismic performance of low-rise masonry buildings due to the prevalence of their construction. Physical tests include scaled and full-sized shake table testing of single-storied and multi-storied structures. Data from instrumented buildings has been collected after major earthquakes and has been analyzed to better understand the seismic response of these masonry structures. Numerical models have also been developed to better predict the seismic behavior of these buildings. Following is an overview of recent and important studies in this field.

Bruneau (1995) published a report on the performance of masonry structures during the 1994 Northridge California earthquake. This document is an overview of the damage sustained by URM structures during the Northridge event. It was observed that out-of-plane wall failures were numerous. These failures were attributed to the wall to roof anchorage being insufficient. Other problematic behavior of masonry structures included pounding of the wood roof joists on the walls and separation of stack bond panels. Older URM buildings were completely ineffective in distributing lateral load into their foundations due to incomplete load paths in the buildings, which was primarily due to inadequate connection between the wall and the diaphragm.

2.1.1 Prior research using test specimens

Prior to this research, scaled shake table tests and an analytical model of low-rise masonry buildings with flexible diaphragms were conducted by Gregory Cohen (2001). This test was conducted for the United States Army as part of a project to ensure the safety of important installations during

seismic events. Two half-scale shake table tests were conducted at UT: one with a wood diaphragm, the other with a roof constructed of 22 gage metal deck. An analytical model was developed using shell elements. The results of the model were in agreement with the results of the physical specimen tests. Data from the shake table tests showed that the shear walls do not govern the seismic response of the building. Out-of-plane wall behavior was shown to be much more dependent on in-plane diaphragm effects than behavior of the shear walls. This research concluded that further studies into the seismic response of low-rise masonry buildings should focus on the effects of diaphragm flexibility on the overall behavior of the structure.

In his dissertation, Cohen (2004) reported on tests of low-rise masonry buildings and evaluations of existing structures. This test was a continuation of the research previously published in 2001 for the US Army. As part of the analysis, Cohen developed a simple method for determining the seismic response of a building by modeling it as a single degree-of-freedom structure. This degree-of-freedom was governed by the flexibility of the roof diaphragm. Results confirmed that this method was accurate in predicting the seismic response. Further testing consisted of shake table tests and quasi-static diaphragm tests. Cohen concluded that the seismic response of low-rise masonry structures with flexible roof diaphragms is dependent on diaphragm flexibility, which can be modeled as a single degree-of-freedom. This conclusion was used when designing the diaphragm models used in the study described in this thesis.

In a Master's Thesis, Yi (2004) presents a study performed on low-rise masonry buildings with flexible diaphragms. Two, scaled unreinforced masonry (URM) specimens were tested under quasi-static loading, and comprehensive non-linear analytical models were developed. This study cataloged the performance of these buildings in order to determine the risk to existing structures, should an earthquake occur. This study also concluded that to model the cracking of masonry walls non-linear

material properties can be used. The models used for the research described in this thesis implemented non-linear material properties to model masonry walls.

Shedid et al. (2009) tested the behavior of fully grouted concrete masonry shear walls. Failure mechanisms, yield behavior, and drift of the wall were studied under lateral load. This report was completed in order to generate data that would help code writers to improve design requirements on concrete masonry unit (CMU) walls.

Most recently, a comprehensive study was completed on concrete masonry walls and full size buildings, which was described in the report, "Performance Based Design of Masonry and Masonry Veneer" (Klinger et al. 2010). This was a joint study completed at Washington State University, University of Louisville, the University of Texas at Austin (UT) and University of California at San Diego (UCSD). Tests were conducted on in-plane specimens, out-of-plane specimens and a full-scale building. All specimens were constructed with masonry veneer on one side, as the scope of the study included analyzing the response of the veneer. Dynamic shake table tests were conducted at UCSD and showed that the in-plane shear walls governed the seismic response of the structure. Rigid response was observed in the shear walls and was characterized by flexural deformation at design level earthquakes and base sliding once the maximum considered earthquake was exceeded. The out-of-plane walls responded as flexural plates, with the foundation, roofs and shear walls acting as boundary elements. Quasi-static testing was conducted at UT by Seongwoo Jo (2010). Quasi-static testing yielded results in agreement with dynamic testing. Additionally, it was determined that the veneer did not increase the stiffness of the walls; it only acted as added mass. The non-linear behavior of the in-plane walls was predicted very well by analytical models by using flexural hinges. This report concluded that concrete masonry structures could experience design level earthquakes without collapse when designed to

current standards. Data from these studies was used to validate the models used for the research described in this thesis.

2.1.2 Prior research using analytical models

In the paper titled "Seismic Evaluation of Unreinforced Masonry Structures with Flexible Diaphragms", Tena-Colunga (1992) presents a linear-elastic multi-degree-of-freedom finite element model that was able to predict the seismic response of an instrumented building. A URM building in Gilroy, CA was instrumented, and the dynamic response of the structure was recorded during the Loma Prieta Earthquake. The primary means for deformation within the model were the diaphragm deflection and shear wall rotation. With these two parameters properly modeled, the response of the URM building was predicted with good agreement. Both the model and the data from the building showed that ground motions were amplified by a factor of 1.45 at the height of the roof diaphragm. This paper provides a background into previous finite element modeling of low-rise masonry structures.

Further data from the 1989 Loma Prieta Earthquake was used by Tena-Colunga and Abrams (1996) to evaluate the seismic response of URM buildings. Data from three instrumented buildings were collected and analyzed using the same analytical model that was presented in 1992 (Tena-Counga, 1992). Analytical studies were conducted in order to compare the effects of flexible vs. rigid diaphragms. Tests showed that the natural period of the structures was considerably longer when a flexible diaphragm was modeled when compared to results using a rigid diaphragm model. It was also shown that flexible diaphragms caused greater out-of-plane wall deflection and experienced higher accelerations. This concept of seismic response controlled by the diaphragm stiffness was used to verify the correct behavior of the finite element models described later in this thesis.

Further tests were conducted by Costley and Abrams (1995) and produced results in agreement with what had been previously determined. For this study, two scaled two-story specimens were tested

on a shake table and analytical models were also developed. Results showed that ground motions are amplified at the roof level and these diaphragm displacements increase wall displacements perpendicular to the wall. This behavior was also observed in the finite element models used in the research described in this thesis. Also provided in this report is a detailed list of prior research into masonry structures.

2.2 Flexible diaphragms

Due to the complexity of diaphragms, research into their behavior is well developed. Numerous experimental tests on diaphragm specimens have been conducted. Reports on dynamic, quasi-static and analytical testing are readily available. Despite many years of investigation, new methods for analyzing flexible diaphragms are being generated. Following is an overview of diaphragm behavior and a review of recent and pertinent diaphragm tests. The types of diaphragms being considered in this study are constructed from metal deck and timber.

The diaphragm is the most important element in the lateral force resisting system for low-rise buildings. It is important to distinguish whether the diaphragm behavior is flexible, rigid, or somewhere in between, for the construction type considered. The International Building Code (2012) defines flexible diaphragms as having a displacement magnitude at design level loading equal to or greater than two times that of the shear walls that they transfer load into. The in-plane flexibility of timber and metal deck diaphragms significantly influences the seismic response of a building. Behaviors affected include in-plane shear forces, chord forces, deflection, and natural period. The deflection, in turn, affects the demand placed on the connection between the diaphragm and the walls of the building that are oriented perpendicular to the loading. It is extremely important to understand diaphragm behavior when considering the lateral performance of a building.

2.2.1 Timber diaphragms

Timber diaphragms are comprised of wood framing: beams or trusses, plywood or Oriented Strand Board (OSB) sheathing and nails. Examples of an unblocked and a blocked timber diaphragms are presented in Figure 2.1 and Figure 2.2.

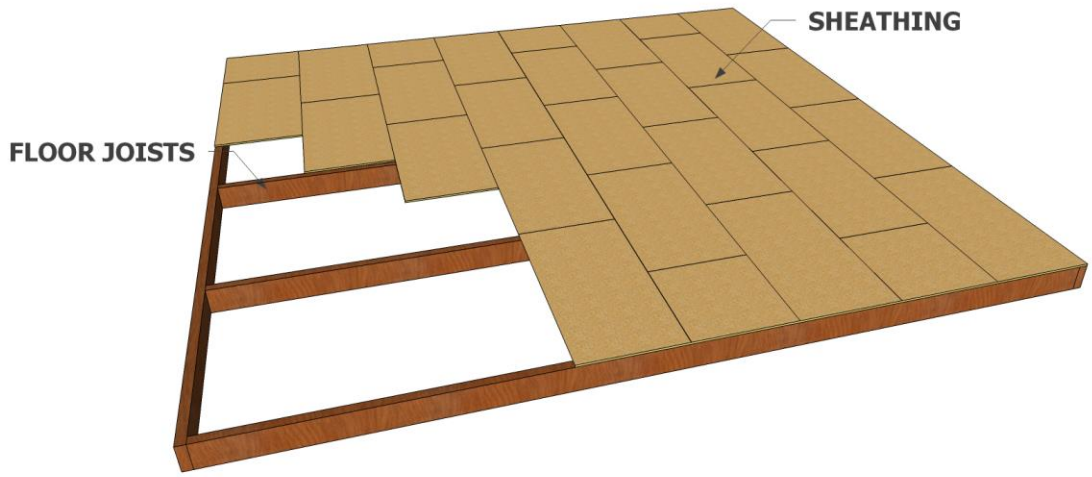

Figure 2.1 Unblocked Wood Diaphragm

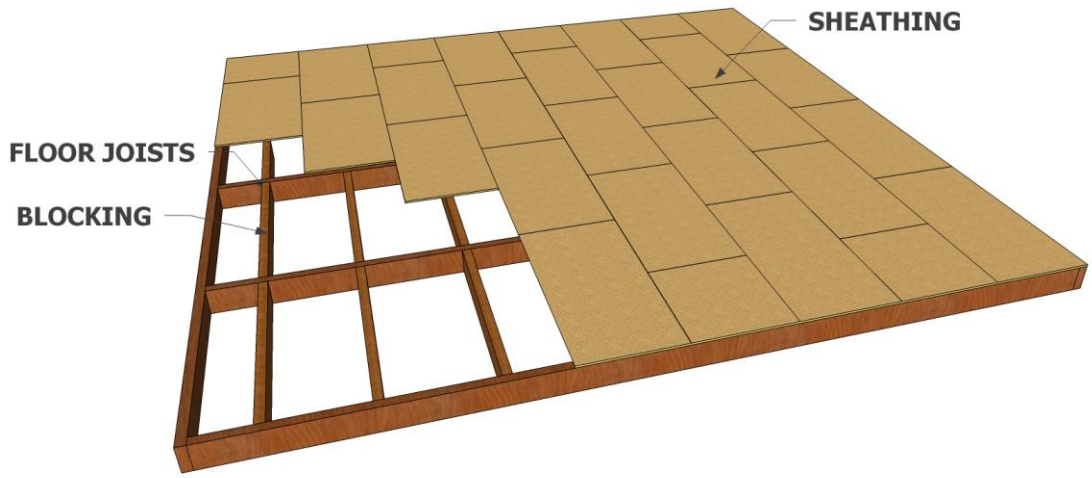

Figure 2.2 Blocked Wood Diaphragm

. Tissell and Elliot (2004) published a report that developed guidelines for designing high shear demand diaphragms. These tests were performed on plywood diaphragms and studied the effects of

specific construction parameters on the overall shear strength. This report confirms that equations for diaphragm capacity are applicable at high shears. To increase wood diaphragm shear capacity, a designer can do any of the following: This research provides an overview of diaphragm behavior and what influences it.

1: Increase nailing

2: Double the amount of sheathing in high shear areas

3: Use pneumatically driven nails

4: Use gluing in the field

5: Design for weakness around openings

The effects of wood diaphragm construction parameters on the diaphragm stiffness were evaluated by Bott (2004). Six specimens were built with various types of construction differences including: walls, glues, openings, chords and blocking. Each diaphragm was tested within the linear-elastic range from which the shear and flexural stiffness were determined. From these tests it was concluded that blocking between the framing had the greatest effect on the diaphragm stiffness. Openings in the diaphragm cause torsional irregularities, which must be accounted for in design. Perimeter walls act as part of the chord element and increase the flexural strength. It was also shown that shear stiffness has a greater effect than flexural stiffness on overall diaphragm behavior. Data from this study was used to validate the finite element models used to complete the research described in this thesis.

Due to their complexity, determining wood diaphragm deflections is very difficult. Skaggs and Martin (2004) published a report on methods for estimating wood diaphragm and shear wall deflections. The report reflects on problems in the code at the time, such as the exclusion of OSB and incorrectly determining nail slip. Correctly estimating deflection is necessary in order to understand and

classify the behavior of a diaphragm. This research provided important background information the on diaphragm deflection for developing finite element models used in the research used . Deflections are estimated by considering four different parameters:

1: Frame element bending

2: Shear deformations

3: Nail slip

4: Chord splice elongation

Data from early wood diaphragm tests is readily available. In 1952, Countryman conducted an investigation on the influence of various construction parameters on diaphragm behavior. Six, quarter-scale and four full-scale specimens were constructed. It was concluded that nailing and nail strength govern the diaphragm strength. A method was provided for calculating diaphragm deflections. Johnson (1956) also conducted full-scale lateral tests on plywood diaphragms. It was concluded that changing the construction parameters drastically affects diaphragm behavior. For a comprehensive review of early wood diaphragm testing see the bibliography on this subject by Peterson (1983).

2.2.2 Metal diaphragms

Metal deck diaphragms are made of corrugated steel with insulation and built-up roofing on top. Following is an overview of research into metal deck diaphragms. An illustration of a metal diaphragm is shown in Figure 2.3.

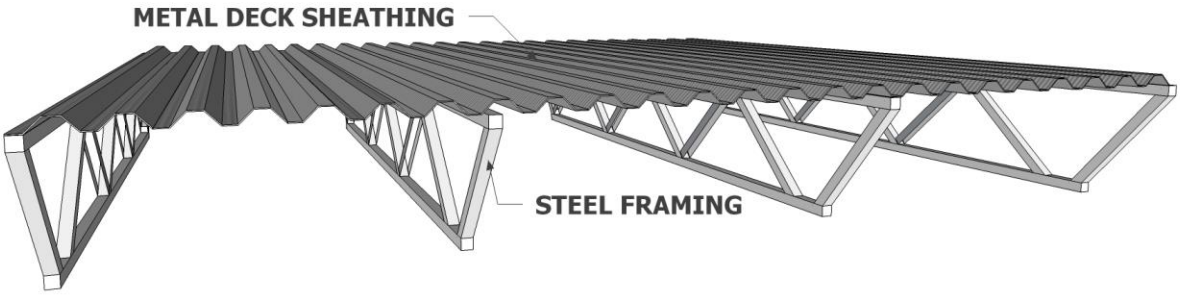

Figure 2.3 Metal Deck Diaphragm

Luttrel (1967) conducted an experimental investigation of strength of light-gage steel diaphragms. Further tests were conducted by Luttrel and Ellifritt in 1970. From these studies several conclusions were made about the behavior of steel diaphragms. Frame member flexibility has a low influence on the ultimate strength of the diaphragm. A direct relationship exists between the number of fasteners on a panel overlap and shear strength. Panel overlap width also has a heavy influence on diaphragm strength. Reversed cyclic loads reduce ultimate shear strength; therefore, ultimate strength calculations using monotonic loads are non-conservative. Increasing steel sheathing strength has a small effect on overall strength of the diaphragm; a 40% increase in the material strength results in a 10% increase in diaphragm strength. Design charts were provided for strength and stiffness of this type of diaphragm, as well as modification factors for various construction parameters.

Robert Tremblay has produced numerous studies on the behavior of steel deck diaphragms. One study reports on 18 large-scale tests using quasi-static load (Essa et al. 2003). This report is significant because it is the first to use quasi-static cyclic load. Three types of connectors used in metal diaphragms

were tested: button pinched, welded, and lap connections. This study showed that overall strength is primarily controlled by connector design. Diaphragm equations were shown to be applicable when connector displacement was less than 10mm. This study also demonstrated that monotonic testing could overestimate ultimate capacity and design values based on monotonic test results need to be adjusted.

Investigations concerning the connectors used to construct diaphragms have also been reported. Rogers and Tremblay (2003) investigated the seismic response of connectors in steel roof deck diaphragms. This investigation was performed because very little data on fastener response to dynamic loads was available. The energy dissipation of the fasteners was tested and hysteresis curves were developed. The tests showed that using dynamic loads to predict diaphragm performance is conservative. Screws were observed to dissipate energy well when displacements were less than 5 mm. Welded connections improved the performance of thin sheet diaphragms.

2.2.3 Prior research using analytical models

Many analytical models have been developed to determine the behavior of flexible diaphragms. Rafik Itani published several papers covering analytical studies on this topic. Itani and Cheung (1984) present a finite element model for estimating wood diaphragm behavior. This model is composed of three types of elements: beam, joint, and plate elements that are used to model frame members, nails and sheathing respectively. Joint elements are modeled with a spring pair assigned a stiffness matrix that correlates to nail stiffness properties. This model was validated with full-scale diaphragm tests. Falk and Itani (1989) published a report with the results of analytical tests using the model developed by Itani and Cheung to investigate the diaphragm requirements in the Uniform Building Code. These tests evaluated the effect of construction parameters on the stiffness of the diaphragm. It was found that blocking affected the stiffness the most due to the additional framing and nailing. Decreasing perimeter nail spacing also had a dramatic effect on the stiffness while field nailing did not. Increasing the strength

of each nail had a small effect on stiffness. All of these parameters were less effective at changing diaphragm stiffness at higher shear loads, due to the non-linear behavior of wood diaphragms. He and Li (2012) published a report in which analytical models and experimental tests were conducted, the same conclusions were reached. It was also shown that frame member spacing had very little effect on diaphragm stiffness.

Judd and Fonseca (2005) developed an analytical model for sheathing to framing connections in wood diaphragms. Like prior analytical models, the connectors were modeled with spring pairs. The spring pairs were shown to be more robust than single spring models when using dynamic loads.

The aforementioned previous research into diaphragm behavior using finite element models develops an understanding of how low-rise masonry structures can be modeled. The models described in this thesis do not employ methods similar to those used in the models described above. However it is important to understand the history of finite element modeling in this area.

2.3 Wall to roof anchorage

Many studies on the behavior and capacity of wall-diaphragm connections have been completed. While data is available on the connection capacity, there is very little data on the effect of diaphragm stiffness on the connection. An overview of investigations into anchorage capacity is provided in the following paragraphs.

The Masonry Standards Joint Committee (MSJC) (2011) provides design procedures for anchor bolts embedded in masonry and masonry grout. Equations to determine the breakout capacity of anchor bolts are provided for allowable stress design and strength design. It is noted that bolt straightening and breakout has only been observed under cyclic loads. Section 5.8.3 requires that bolts are to be at least 0.5 in. in diameter, spaced at a maximum of 6 feet, and embedded to a minimum of 15 in (MSJC 2011). These standards were used when creating the finite element models used in this thesis.

Shear capacity of anchor bolts in masonry have been investigated by Brown and Whitlock (1983) and Ueda et al. (1990). These papers outline the breakout capacity of anchor bolts under shear and combined tension and shear. Parameters including embedment length and edge distance are discussed. For the model used to complete the study presented further in this paper, data from Brown and Whitlock's report was used.

An overview of previous research into the wall/diaphragm connection is provided here for the reader. The following discussion will provide insight into the progression of knowledge obtained on this connection type.

Hatzinikolas et al. (1983) reported on an investigation on drilled-in inserts used in masonry construction. This report outlines the shear and tensile strength of bolts placed into bored holes in masonry units. Graphs and tables outline the non-linear behavior of these connectors.

Tensile strength of anchor bolts embedded in the tops of CMU walls was investigated by Weigel et al. (2002). Tests prior to this had focused on anchor bolts embedded into the face of CMU blocks. This report provides design parameters for edge distance for anchor bolts in the tops of CMU walls. All anchor bolts were embedded 4 inches into the grout and were found to meet tensile strength requirements for the 2002 MSJC code. For a comprehensive list of research into tensile strength of anchor bolts in the face of concrete masonry the reader is referred to the literature review provided in this publication.

Older masonry wall connections were investigated by Lin and Lafave (2012). These connections were typically straps nailed to the wood joist, bolted though the wall, and anchored to a plate on the exterior of the veneer. These connections exist only on joists perpendicular to the wall, and therefore do not have a good lateral load path. This report includes force-deflection curves for older connections.

Karim et al. (2011) produced a study that provided the wood capacity of a wall/roof connection. This study was conducted because the wood elements may be the weakest element of the entire connection, and therefore govern capacity. From the data gathered, equations are provided to determine the capacity of these connections.

3.0 Model Validation

This chapter outlines the methods and procedures used to complete this study. Each section describes the procedure used to validate each component of the model used in the parametric study.

In order to ensure the accuracy of the model, its components were verified against physical test data. These data were taken from several sources that are discussed in detail within further sections. The roof diaphragm, shear walls, and out-of-plane walls were each verified separately. Only the behavior of each of the elements as a whole is important for the purposes of the model. The models did not consider the effects of individual components of a structural system such as; nails, sheathing, and framing. For this reason, each element in the lateral force resisting system was modeled as a shell. The use of shell elements allowed the model to be use material properties that that define the behavior of a complete structural system. Shell elements were given stiffness properties that represent the equivalent stiffness of each element type as a whole. The effects of individual components such as nailing or reinforcing steel were ignored. Since shell thickness did not change for each model, only the material properties influenced results. Therefore, all efforts to calibrate and verify each model focused on determining material properties that would generate agreeable results with physical test data. These material properties did not necessarily correspond to realistic values for the materials being modeled, but were effective material properties that worked within the parameters of the finite element model. Following are the processes with which each structural element was calibrated then validated.

3.1 Diaphragm

The finite element used to model the diaphragm was a 4-node, 6-degree-of-freedom linear-elastic shell. Linear behavior was determined to be adequate because non-linear deformations are not typical in the diaphragm when design level loads are being considered. SAP2000's thick shell elements were selected in order to include the effects of shear deformations. The shell depth was set to 12 inches to model the typical depth of wood diaphragm framing members. Each shell was assigned an isotropic

material property due to the unidirectional load being applied. It is fully recognized that diaphragms typically behave as orthotropic elements when 2-D or 3-D loading is considered, due to the directionality of the sheathing orientations and inter-panel bearing that occurs.

The diaphragm model was calibrated by using test data from two different studies. The first were gathered by Bott (2004). The results of the test used from the Bott tests were stiffness properties: *EI* and *GA*. *EI* defines the in-plane flexural stiffness of the diaphragm and *GA* defines the in-plane shear stiffness. The diaphragms tested were constructed of wood in several different configurations. For the purposes of this model the selected configurations reflected the most common diaphragms seen in the construction of "big box" stores and warehouses being analyzed. The selected diaphragms consisted of the specimens with chords, were fully sheathed, and used nailed connections to attach the sheathing to the framing. Data from both blocked and unblocked specimens were used for validation. Specimen one measured 20'x16' and was loaded on the 20' side. Specimen six was a 40'x10' and was loaded on the 40' side. Selected tests and results from Bott's data are presented in Table 3.1.

Table 3.1. Bott Test Data Used For Model Calibration

Test	GA (kips)	EI (kips-in^2)
Specimen 1 test 7	3091	$66.3*10^6$
Specimen 6 test 4	764	$80.2*10^6$

To input material stiffness into SAP2000 *EI* and *GA* were converted into *E* and *G*, where *E* is the modulus of elasticity, *I* is the moment of inertia, *G* is the shear modulus, and *A* is the cross sectional area of the diaphragm. To do this, the shell section properties were first determined. Once the section geometry was determined, *I* was calculated. The modulus of elasticity, *E*, was then calculated by dividing *EI* by *I*. *G* was calculated by assuming a Poisson's ratio of 0.45. This Poisson's ratio is typical for wood.

Small adjustments were then made to *E* in order to generate better results, when the model predictions were compared to the actual diaphragm test data.

The second study used for model calibration was from Duncan and Dolan (2012). This data was generated from two diaphragm specimens measuring 24'x24'. The data consisted of load and displacement over time. Each diaphragm specimen was loaded with two actuators, identified as the North load and South load. Material properties for these diaphragms were determined by first using the *E* from Bott's data, then making adjustments until the error between the predicted and test displacements was acceptable. *G* was calculated with Poisson's ratio assumed to be 0.45. Selected test results from the Duncan and Dolan data are presented in Table 3.2.

Table 3.2. Duncan and Dolan (2012) Test Data Used for Model Calibration

Test	South Load (lb)	North Load (lb)	Center Deflection (in)
Specimen A	9032	8472	0.418
Specimen B	10746	9933	0.479

To validate each model correctly, specific boundary conditions and load parameters were met. Displacement restraints parallel to the load were applied at the nodes on the corners of the side the load was applied on. Each joint along the centerline parallel to the load direction had displacements restrained perpendicular to the load direction. Joints along the line of the applied load were loaded with a fraction of the applied load. This fraction was equal to the total load divided by the number of nodes along the load line. Although Bott and Duncan and Dolan used a cyclic load protocol , only static maximum and minimum experimental loads were used to validate the model. This is because the model simulation did not include the plastic range of displacements of the diaphragms. Applying only the extreme loads to the model was sufficient to replicate the elastic behavior of the physical tests. In order

to improve accuracy, the shell was discretized into 1'x1' elements. The diaphragm model with restraints is shown in Figure 3.1.

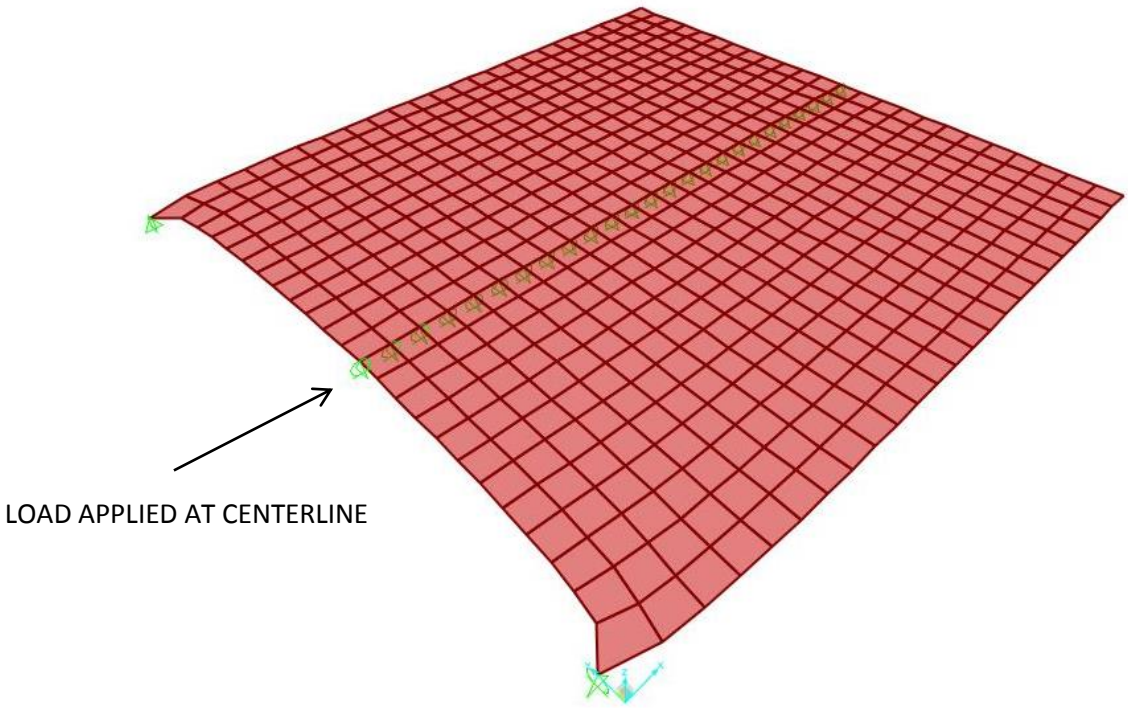

Figure 3.1. 3D View of Diaphragm Calibration Model

Each selected specimen listed was modeled with this method. The results of each model and corresponding shell stiffness properties are presented in Table 3.3.

Table 3.3. Bott Diaphragm Model Calibration Results

Test	Test Disp. (in)	Model Disp. (in)	Error (%)	E (ksi)	G (ksi)
Bott Specimen 1 Test 7	0.2094	0.2057	1.767	16.0	5.51
Bott Specimen 6 test 4	0.8169	0.8178	0.104	9.5	3.279
Duncan and Dolan Specimen A	0.45	0.4535	0.778	13.25	4.569
Duncan and Dolan Specimen B	0.479	0.474	0.981	14.8	5.086

In order to determine a set of material properties that considered a range of diaphragms, the average of Bott's Specimen 1, Test 7, and both of the Duncan and Dolan specimens were used. Bott's Specimen 6, Test 4, was not used because its aspect ratio was very different from the others. Each model material property that was averaged was then reanalyzed using the new properties. The simulation errors of each considered test using the averaged material properties are presented in Table 3.4.

Table 3.4. Diaphragm Results Using Averaged Material Properties

Test	Test Disp. (in)	Model Disp. (in)	Error (%)	E (ksi)	G (ksi)	Nu
Bott S1T7	0.2094	0.2244	7.163	14.65	5.056	.45
Duncan and Dolan SA	0.45	0.4097	8.956	14.65	5.056	.45
Duncan and Dolan SB	0.479	.0477	0.418	14.65	5.056	.45

From these results it was clear that the averaged material properties were effective in modeling the test data with agreeable accuracy. Thus, using these properties with the shell elements previously described was a sufficiently accurate method of modeling diaphragm behavior.

3.2 Out-of-plane walls

To calibrate the stiffness of the out-of-plane walls, a 4-node, 6-degree-of-freedom non-linear shell element was selected. SAP2000 contains a layered, non-linear shell element that uses material properties to determine non-linear behavior. It was necessary to use non-linear shells to model the out-of-plane walls due to the high deflections and non-linear behavior they exhibit in design level earthquakes. In order to include the effects of shear deformation SAP2000's thick shell properties were enabled. Isotropic material properties were used because of the unidirectional load applied.

To determine the non-linear material properties of the out-of-plane walls, data from the University of Texas (UT) (Jo 2010) was used. The results of the tests were displacements due to a cyclic load on each specimen, an example of which is shown in Figure 3.2. UT tested three specimens: UT CMU1, UT CMU 2, and UT CMU 2 MC. Each of these specimens was constructed of 8" light-weight CMU and measured 8'x8'. Each wall was fully grouted. On one side of the CMU wall, a brick veneer was constructed. Both sides of the wall were instrumented during the test, but for this study only data from the CMU side was used.

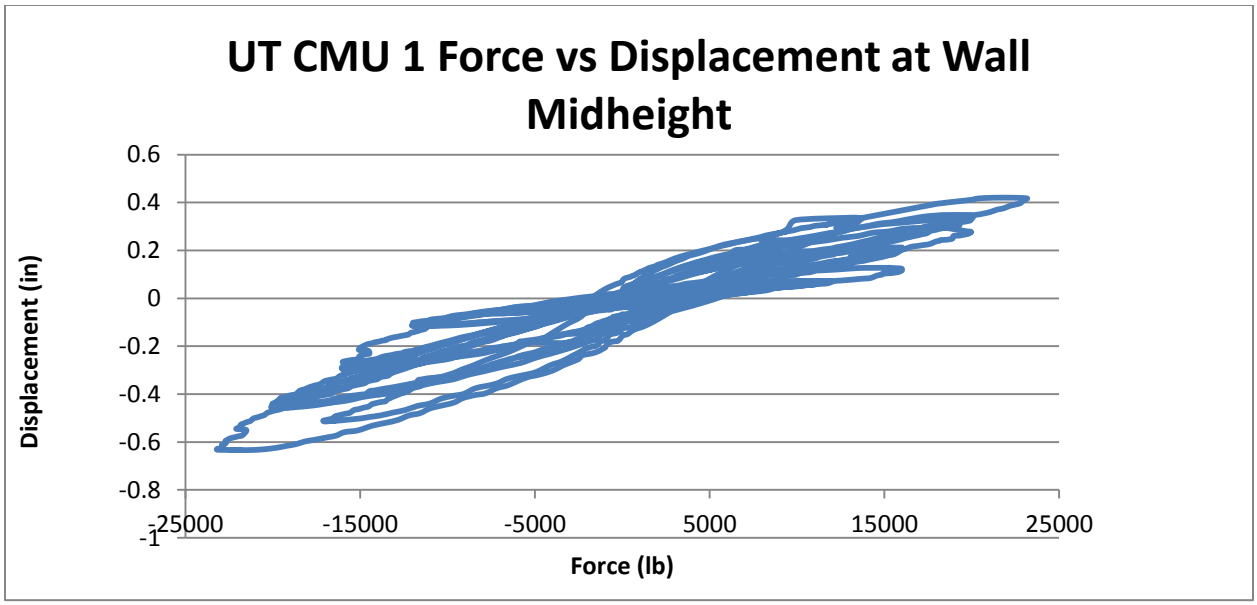

Figure 3.2. UT CMU 1 Data

The non-linear material properties of the out-of-plane walls were calculated by assuming the test specimens behaved as simple beams. The boundary conditions used in the UT tests were consistent with this assumption. To model the data shown in Figure 3.2, a bilinear curve was used. To determine the curve, the initial modulus of elasticity (*E*) representing the linear-elastic range was calculated then used to determine an *E* for the non-linear range. From the given deflection data E was calculated using the simple beam moment formula. Stress and strain were then determined from the calculated moment

and *E*. By using the ratio of the linear to non-linear slopes of the load-displacement curves, the value for the non-linear *E* was determined. These calculations assumed out-of-plane flexure governed the behavior of the walls, an assumption which was validated when later comparing the model output to the UT test results. These calculations were completed for each specimen then averaged to obtain the final non-linear stress-strain curve that was input into SAP2000. This stress-strain relationship is presented in Figure 3.3 and Table 3.5.

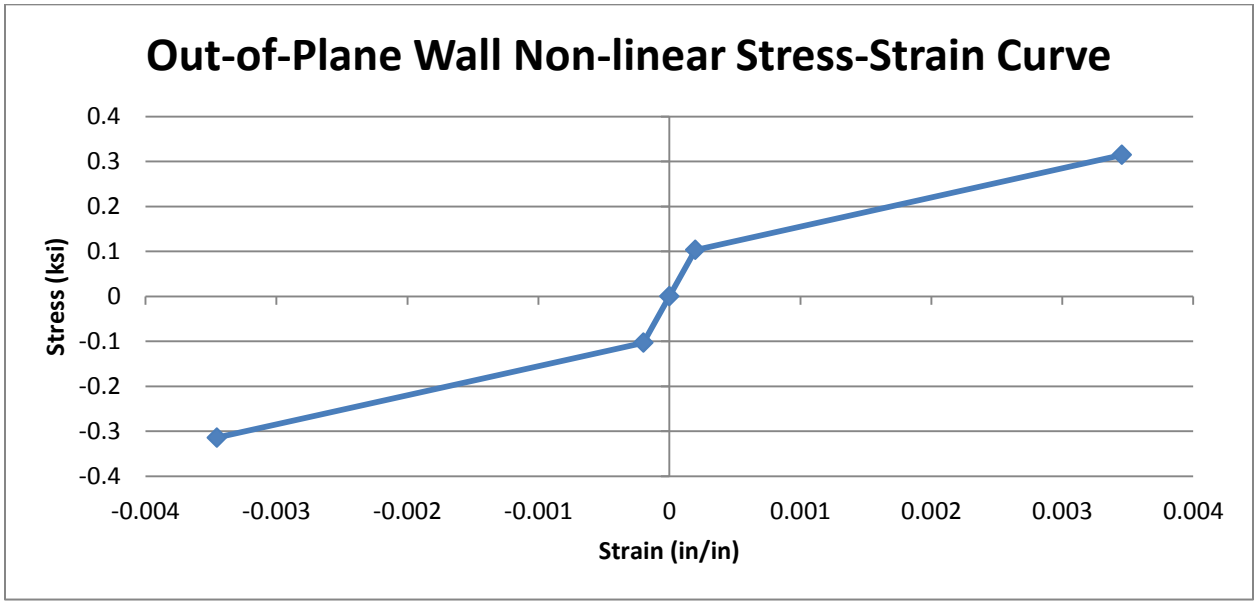

Figure 3.3 Stress-Strain Curve for Non-Linear Out-of-Plane Walls

Table 3.5. Stress-Strain Values for Non-Linear Out-of-Plane Walls

Strain (in/in)	Stress (ksi)
-0.003455	-0.31442
-0.000198	-0.10319
0	0
0.000198	0.10319
0.003455	0.31442

To model each specimen, an 8'x'8' wall was constructed in SAP2000. It consisted of the aforementioned shell elements that were then defined to be 8" thick. This thickness was selected to match the thickness of the physical specimens. Boundary conditions for the calibration model consisted of pins at the bottom and rollers at the top. Loads were applied as a surface pressure time history. Each time history was specific to the UT specimen being modeled. An elevation view of the wall model is shown in **Error! Reference source not found.**.

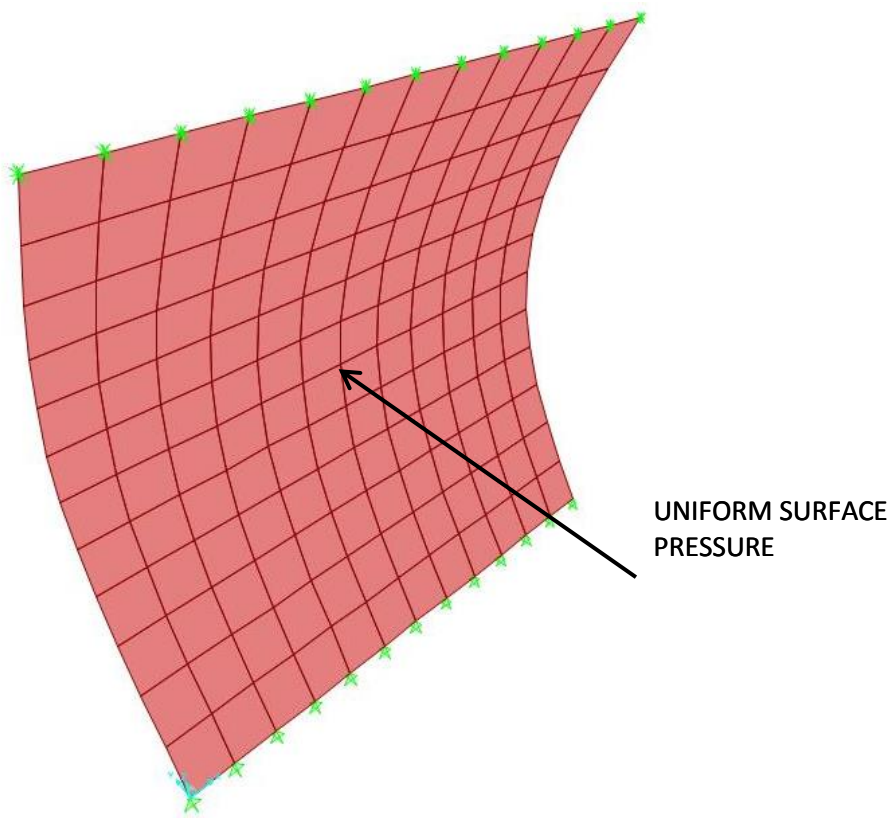

Figure 3.4 Elevation View of Out-of-Plane Wall Calibration Model

The comparisons of the UT data and of the deflections predicted by the model using the averaged stress-strain values for each specimen are presented in Figure 3.5 through Figure 3.7.

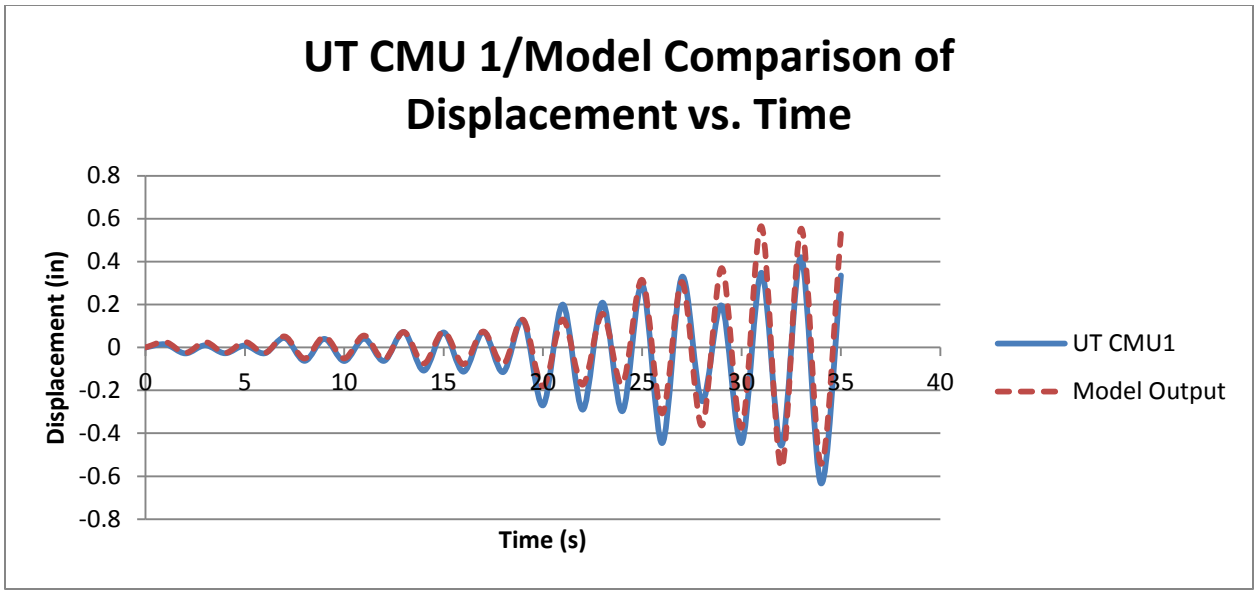

Figure 3.5. UT CMU 1/Calibration Model Comparison

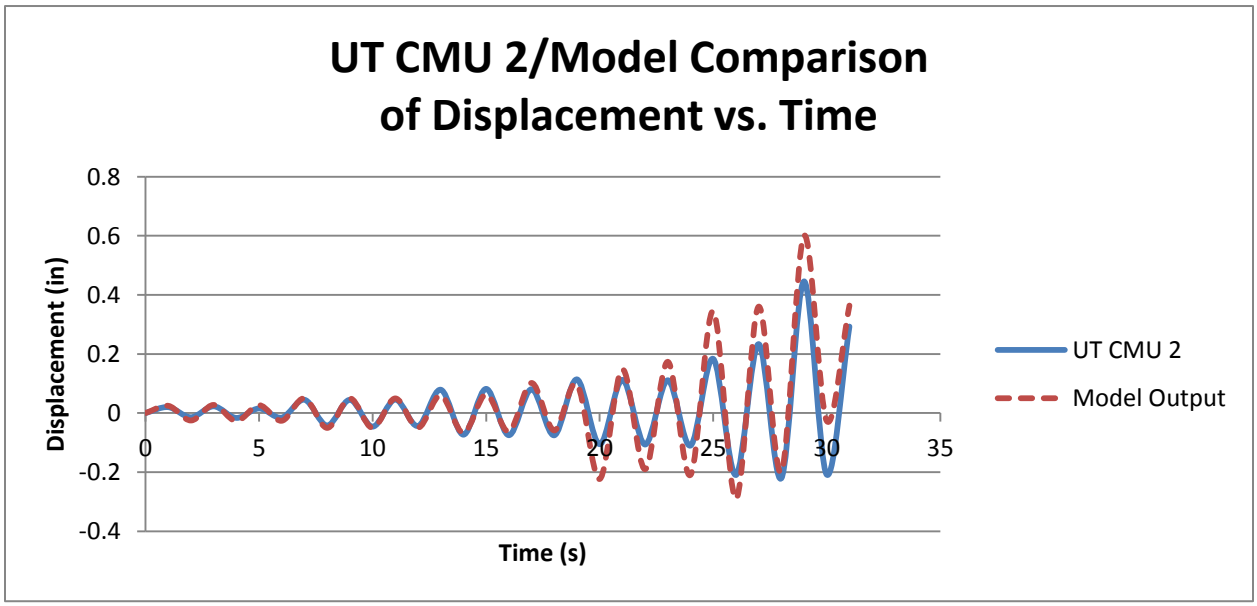

Figure 3.6. UT CMU 2/Calibration Model Comparison

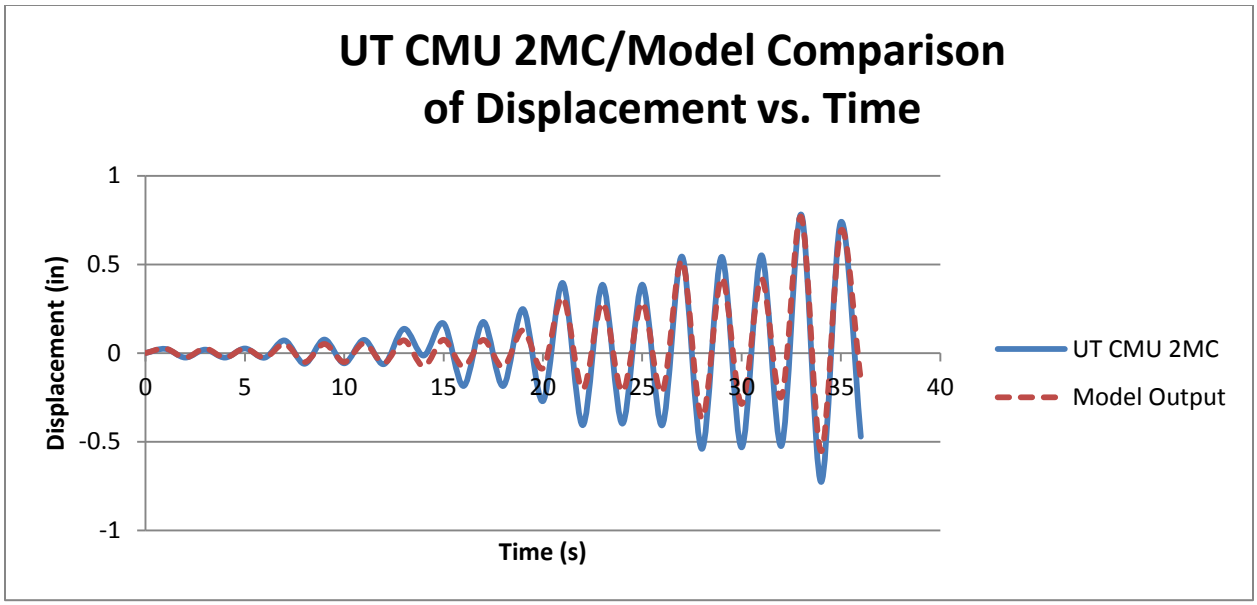

Figure 3.7. UT CMU 2 MC/Calibration Model Comparison

From these graphs it is shown that the stress-strain values calculated are reasonably accurate in predicting the non-linear behavior of the out-of-plane walls and are acceptable for use in the complete building model.

3.3 Shear walls

A 4-node, 6-degree-of-freedom linear-elastic shell element was selected to model the in-plane wall behavior. Linear behavior was determined to be appropriate for this model because non-linear behavior is not expected in the shear walls at the design level earthquake. SAP2000's thick shell properties were selected in order to include the effects of shear deformations. Isotropic material properties were used because of the unidirectional load applied. Out-of-plane behavior of the shear wall elements is out of the scope of this study and therefore was restricted.

The shear wall models were calibrated using test data from The University of Texas (UT) (Jo 2010). These tests were quasi-static cyclic and were conducted on 2 different specimens. The results of

these tests were non-linear load-deflection curves that were used to obtain material properties for the SAP2000 model. Only the linear portion of these curves was used to calibrate the shear wall models. These specimens were 4'x8' and constructed of lightweight 8"x8" fully grouted CMU. On one side of the CMU wall a brick veneer was constructed. Both sides of the wall were instrumented during the test, but for this study only data from the CMU side was used because the seismic response of the veneered masonry wall was not of interest. To determine the linear-elastic material properties of the wall, the load and deflection at the yield point were selected for both the positive load and negative load. Selected tests and results are presented in Table 3.6.

Table 3.6. University of Texas Shear Wall Data

Test	Load	Load (lb)	Deflection (in)
UT CMU 3	Positive	6428	0.0731
UT CMU 3	Negative	5660	0.0733
UT CMU 4 MC	Positive	4435	0.0331
UT CMU 4 MC	Negative	4749	0.0375

To model each test specimen correctly, specific boundary and load conditions were met. The bottom of the wall was pinned at each joint and the top was restrained out-of-plane. The model was discretized into 1'X1' elements. Shell thickness was set at 8" to model the size of the CMU block used. The load observed to cause yielding in the specimens was applied as a traction at the top of the wall. Only this specific load was used because only the elastic range of each test specimen was considered for the model. The shear wall model with restraints is shown in Figure 3.8.

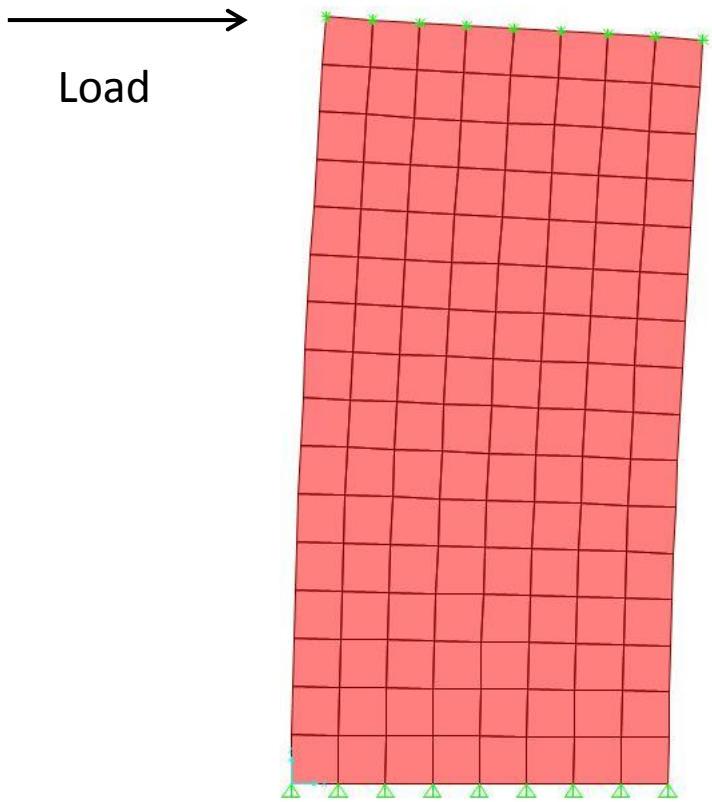

Figure 3.8. Elevation View of Shear Wall Calibration Model

To convert this data into material properties, the deflection equation for flexure of a cantilever beam with a point load at the tip was used. For the considered load and displacement, the equations were solved for the modulus of elasticity *E*. The shear modulus G was calculated by using this value of *E* and an assumed Poisson's ratio of 0.2, which is an approximation for concrete. Once *E* and *G* were determined, a shear wall model was analyzed with the given test protocol. The model predicted deflections were then compared to the test data and the value of E was modified as needed to minimize the error between the two deflections. Table 3.7 contains the material properties determined with this procedure.

Table 3.7. UT Shear Wall Calibration Results

Test	Load	Force (lb)	Disp.	Calculated E (ksi)	Model E (ksi)	Model Disp. (in)	Error (%)
UT CMU 3	Positive	6428	0.0732	351.3	420.0	0.072	1.067
UT CMU 3	Negative	5660	0.0733	308.9	365.0	0.073	0.130
UT CMU 4 MC	Positive	4435	0.0331	535.2	625.0	0.034	1.361
UT CMU 4 MC	Negative	4749	0.0375	506.6	600.0	0.038	0.011

After these calibration results were obtained, an average *E* of 502.50 ksi was calculated in order to use a material property that considered a range of tests. This average *E* was then used to reanalyze the model for each specimen. The results of the tests using the averaged properties are presented in Table 3.8.

Table 3.8. Shear Wall Results Using Averaged Material Properties

Test	Load	Test Disp. (in)	Model Disp. (in)	Error (%)
UT CMU 3	Positive	0.0732	0.0605	17.33
UT CMU 3	Negative	0.0733	0.0533	27.39
UT CMU 4 MC	Positive	0.0331	0.0418	26.10
UT CMU 4 MC	Negative	0.0374	0.0447	19.21

Although the percent errors shown in the previous table appear to be significant, the average *E* is considered to be sufficiently accurate to use in the building model because the investigation is focused on the effect of relative stiffness between the diaphragm and the walls loaded out-of-plane and oriented perpendicular to the loading. Also, the error values are high because the displacement values are very small. The largest difference between the model and test data is 0.02 inches. This is insignificant when compared to the displacements of the diaphragm and perpendicular walls, and therefore it is clear that the average material properties calculated for the shear wall model are sufficiently accurate to represent the shear wall behavior.

3.4 Connections

For the purposes of this study, only the connection between the walls and roof diaphragm was modeled. The type of connection simulated was a bolt anchored into the CMU grout that the roof framing members attach to. For this study, data from Brown and Whitlock (1983) was used to calibrate the non-linear link properties. The force displacement curve used from this paper is displayed in Figure 3.9 and in Table 3.9. For the purposes of this study the link has stiffness only in the local shear directions. Axial and bending stiffness of the connection are not directly considered when modeling this connection, but rather the bending action is effectively incorporated into the shear behavior of the bolt.

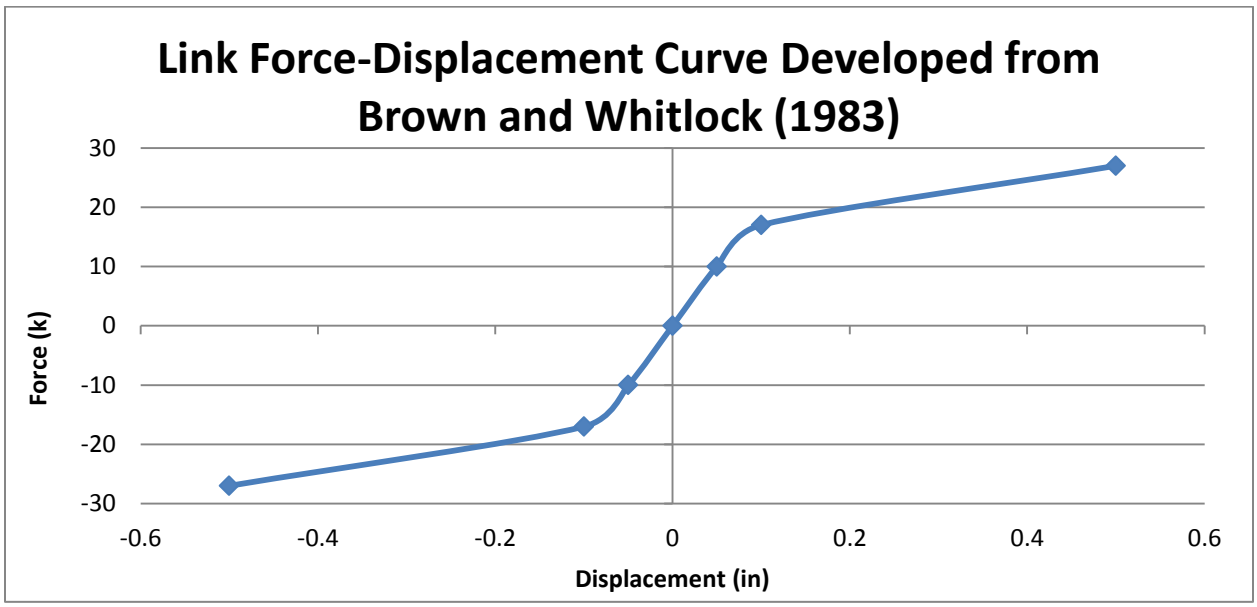

Figure 3.9. Non-Linear Link Force-Displacement Curve

Table 3.9 Non-Linear Link Force-Displacement Values

Displacement (in)	Force (kip)
-0.5	-27
-0.1	-17
-0.05	-10
0	0
0.05	10
0.1	17
0.5	27

3.5 Model Verification Summary

This section summarizes the model properties that were described in the previous sections. Each of these properties has been specifically calibrated for use in this study. All material properties are useful for application only in the models constructed for this study. They do not represent practical material properties for the materials being modeled. Therefore, each property described is an effective stiffness, given the dimensions assumed for the finite elements used for each type of building element. The model properties that were obtained during the calibration phase of this study are shown in Table 3.10.

Table 3.10 Finalized Model Properties

Model Component	Linear Properties			Non-Linear Properties			
	E (ksi)	G (ksi)	v	Stress (ksi)	Strain (in/in)	Force (k)	Displacement (in)
Diaphragm	14.65	5.05	0.45				
In-Plane Walls	502.00	209.38	0.20				
Out-of-Plane Walls				-0.00346	-0.31442		
				-0.00020	-0.10320		
				0.00000	0.00000		
				0.00020	0.10320		
				0.00346	0.31442		
Wall Diaphragm Connection						-0.5	-27.0
						-0.1	-17.0
						-0.1	-10.0
						0.0	0.0
						0.1	10.0
						0.1	17.0
						0.5	27.0

3.6 Mesh density

In order to generate accurate results an appropriate mesh density was selected. Each of the four types of elements: diaphragm, out-of-plane walls, shear walls, and links was tested with a monotonic load. The mesh density was initially very coarse, then refined until the results changed by less than 2%. The diaphragm mesh was tested for two different results: link force and shell element displacement, the

results of which are shown in Table 3.11. The wall elements were tested only for displacement since this is the parameter that produces the forces in the connections. The results of the wall mesh tests are shown in Table 3.12 and Table 3.13. From these comparisons it is clear that a 4'x4' shell element yields sufficiently accurate results. For this study all walls and roofs were modeled with shell elements of this size.

Table 3.11. Diaphragm Mesh Test Results

Shell Size	Shell Disp. (in)	Link Shear Force(K)	% Error Disp.	% Error Shear Force
10'x10'	0.1753	5.323	-	-
5'x5'	0.1756	5.331	0.171	0.150
2.5'x2.5'	0.1761	5.348	0.284	0.318

Table 3.12. Shear Wall Mesh Test Results

Shell Size	Horizontal Disp. (in)	Vertical Disp. (in)	% Error H. Disp.	%Error V. Disp.
10'x10'	0.0034	0.0017	-	-
5'x5'	0.0034	0.0018	0	5.882
4'x4'	0.0035	0.0018	2.941	0
2.5'x2.5'	0.0034	0.0018	-2.857	0

Table 3.13. Out-of-Plane Wall Mesh Test Results

Shell Size	Shell Disp. (in)	%Error Disp.
10'x10'	108.227	-
5'x5'	108.545	0.293
4'x4'	108.6505	0.0971

4.0 Simulation Procedure

This section outlines the procedure used to conduct this study. Detailed descriptions of the finite element models, load protocols, and data collection procedures used for this study are included. These procedures were designed to achieve the goal of quantifying the effect of diaphragm stiffness properties on the force transferred between the wall perpendicular to the load direction and diaphragm.

4.1 Building Models

To complete this study 20 finite element models were constructed. The range of parameters these models incorporated was selected to represent a broad spectrum of feasible construction practices. Four different roof diaphragm aspect ratios were tested. For each aspect ratio, 5 different diaphragm stiffness properties were used. The diaphragm aspect ratio is defined by the ratio of length of the roof parallel to the load to the length of the roof perpendicular to the load (AF&PA §14.4.1.5). The diaphragm stiffness properties used were modifications of the diaphragm property determined during the model verification phase of this study. For each aspect ratio, the height of the building remained constant at 32 feet. The parameters for each model are shown in Table 4.1. The building dimensions shown do not exactly correspond to the aspect ratio selected. This difference was intentional, and served to allow for use of 4’x4’ shell element mesh that was selected during the mesh density study phase of this project.

Table 4.1. List of Parameters for each Model Constructed

Model Number	Roof Diaphragm Aspect Ratio	Roof Diaphragm Dimensions (ft)	Diaphragm E modifier	Diaphragm E (ksi)
1	1:1	52 x 52	0.5	7.325
2	1:1	52 x 52	1.0	14.65
3	1:1	52 x 52	1.5	21.975
4	1:1	52 x 52	2.0	29.3
5	1:1	52 x 52	3.0	43.95
6	2:1	100 x 52	0.5	7.325
7	2:1	100 x 52	1.0	14.65
8	2:1	100 x 52	1.5	21.975
9	2:1	100 x 52	2.0	29.3
10	2:1	100 x 52	3.0	43.95
11	3:1	152 x 52	0.5	7.325
12	3:1	152 x 52	1.0	14.65
13	3:1	152 x 52	1.5	21.975
14	3:1	152 x 52	2.0	29.3
15	3:1	152 x 52	3.0	43.95
16	4:1	200 x 52	0.5	7.325
17	4:1	200 x 52	1.0	14.65
18	4:1	200 x 52	1.5	21.975
19	4:1	200 x 52	2.0	29.3
20	4:1	200 x 52	3.0	43.95

The configuration of each model was relatively simple; each model was made of 4 walls and a roof. Each wall was pinned at the base and connected to the roof diaphragm by non-linear links. To allow space for these links, the roof was vertically offset from the walls by 1 inch. The links spanned this distance. The links were spaced at 4 feet, which matches requirements set by MSJC (2011). The models were constructed with the earthquake load applied in a specific direction. Walls parallel to the load direction were defined by the properties described in section 3.3, Shear Walls. Walls perpendicular to the load direction were defined by the properties described in section 3.2, Out-of-plane walls. An example of a 1:1 aspect ratio model is displayed in Figure 4.1. All other models are similar, the one change being the length of the out-of-plane walls. For each change in aspect ratio only the length of the

out –of –plane walls was changed.

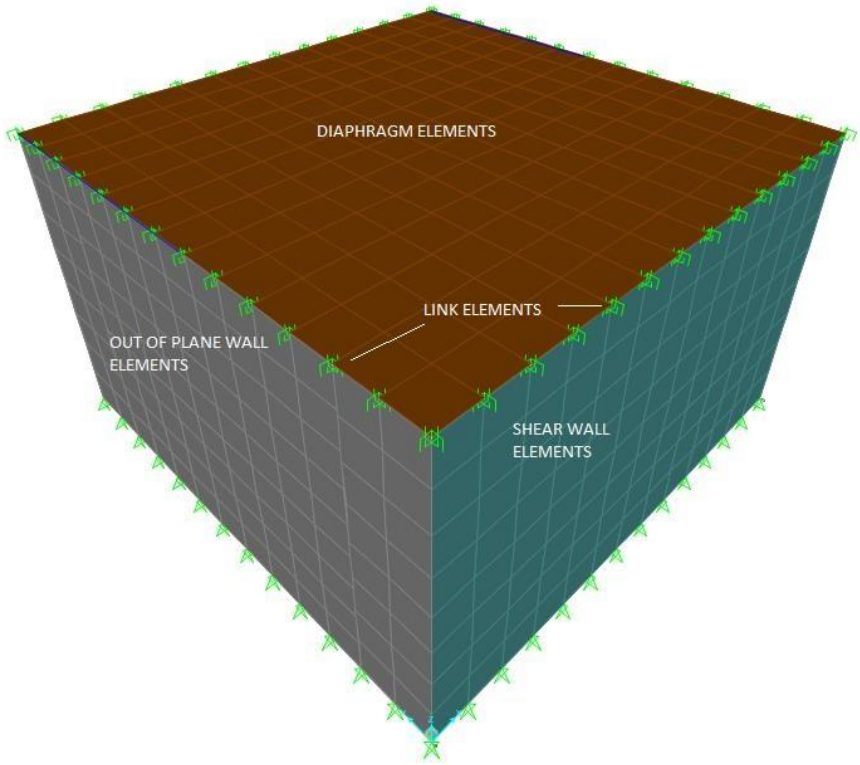

Figure 4.1 Building Model, 1:1

In order to correctly model the desired building activity, several node constraints were applied. All nodes that formed shear wall elements were constrained out-of-plane. Roof diaphragm element nodes were also constrained out-of-plane. The effect of these constraints was to ensure the model experienced displacement only in the direction being considered. A graphic of these constraints is shown in Figure 4.2.

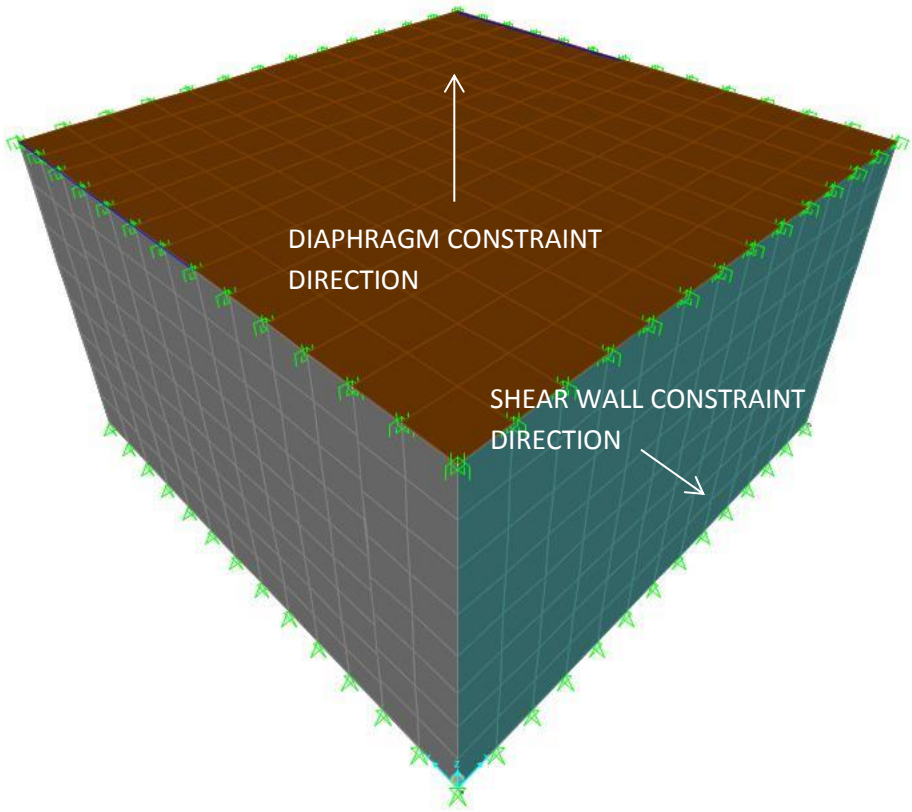

Figure 4.2 Shell Element Constraints

In practical construction, CMU walls are built with bond beams and expansion joints. The specimens used for wall element calibration did not contain these features. To model the bond beams, line elements were developed. The line elements contained no mass and dimensions; they only served to add reinforcement in the areas that bond beams would be present. The reinforcement modeled consisted of 2 standard #5 (5/8-in diameter) Grade 60 steel reinforcing bars. The line element was placed at the top of the walls to model standard construction practices. Expansion joints are constructed to facilitate thermal expansion and contraction of the CMU walls. For this study the expansion joints were only modeled on the out-of-plane walls. An expansion joint was created on each out-of-plane wall 8 feet from the connection with the shear walls. The expansion joint was created by simply meshing

shell segments differently, such that shell elements at the location of the expansion joint did not have shared nodes. In practical construction, expansion joints are located at regular intervals along the wall; this was found to be unnecessary in the building model. Using expansion joints at only 8 feet from each shear wall generated the same results as using expansion joints at regular intervals.

During preliminary testing, it was observed that higher order mode shapes were influencing the models' results. This effect was undesirable as only the fundamental mode shape is expected or observed to occur during a seismic events or shake table tests. In order to minimize this effect, Rayleigh Damping was applied to the higher order modes. SAP2000 allows the user to apply Rayleigh Damping to specific periods and specify the desired amount of damping. The program then computes the damping coefficients and applies the damping. In order to determine the natural period of each mode, SAP2000's modal analysis function was used. All but the fundamental mode were damped. 3% damping was used for all extraneous periods. The fundamental period for each model is displayed in Table 4.2.

Table 4.2 Fundamental Period for Each Model

Model Number	Natural Period (s)
1	0.419
2	0.408
3	0.405
4	0.403
5	0.402
6	0.583
7	0.527
8	0.511
9	0.503
10	0.495
11	0.752
12	0.624
13	0.579
14	0.558
15	0.537
16	0.920
17	0.735
18	0.660
19	0.621
20	0.582

4.2 Load Protocol

For each test, an acceleration time history was used to simulate a seismic event on the building model. Two different acceleration records were selected from the 1994 Northridge Earthquake. One record was taken from the Canoga Park Station and the other was from the Tarzana Station. These records were gathered from the Pacific Earthquake Engineering Research Center website (PEER). Two different acceleration records were used to ensure that the results obtained were not specific to one acceleration record. This data was obtained from the PEER Berkeley website (2014). For the purposes of this study, only the portions of the records up to the largest accelerations were used.

The Canoga Park record used was titled, Canoga Park – Topanga Canyon, 196. The first test performed with this acceleration record used the data between 2.5 and 15 seconds. A second test was

performed using the data from 2.5 to 10 seconds. The second test showed that the maximum acceleration is contained within the shorter period. The data from the 10 to 15 second interval did not change the results since only the maximum displacements and connection forces were of interest. Therefore, to decrease computational time for each model, the acceleration data from 2.5 to 10 seconds was used for the Canoga Park record. The full Canoga Park record and the portion, which was used for this study, are displayed in Figure 4.3. Data showing that the shorter record includes the maximum force on the connection elements is displayed in Figure 4.4.

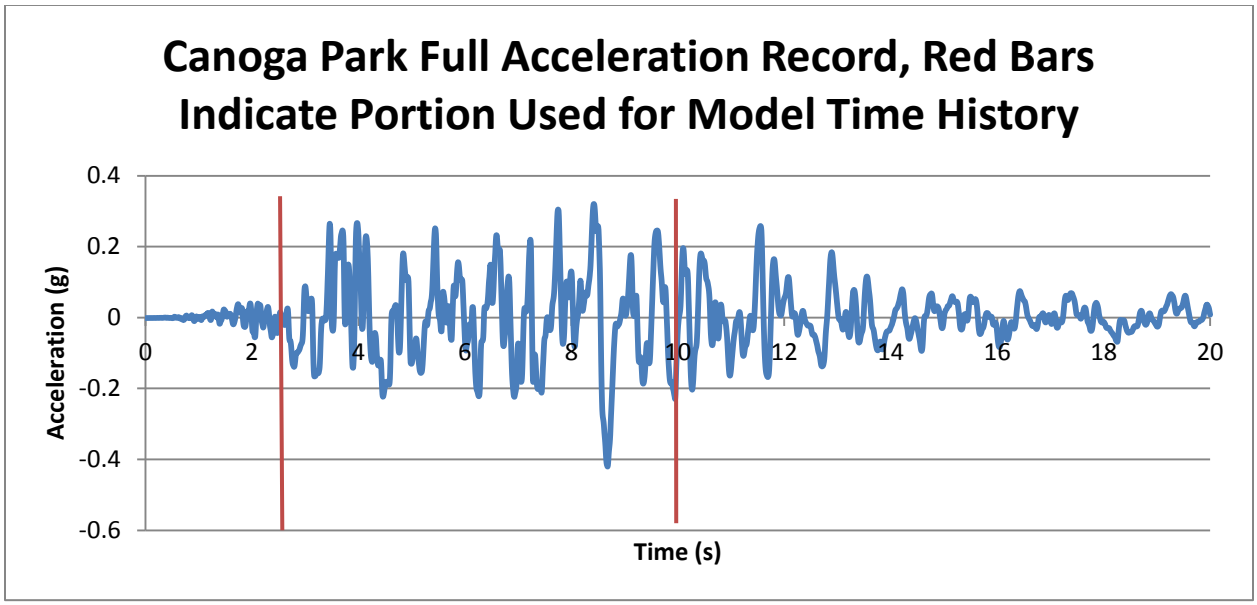

Figure 4.3. Canoga Park Acceleration Record

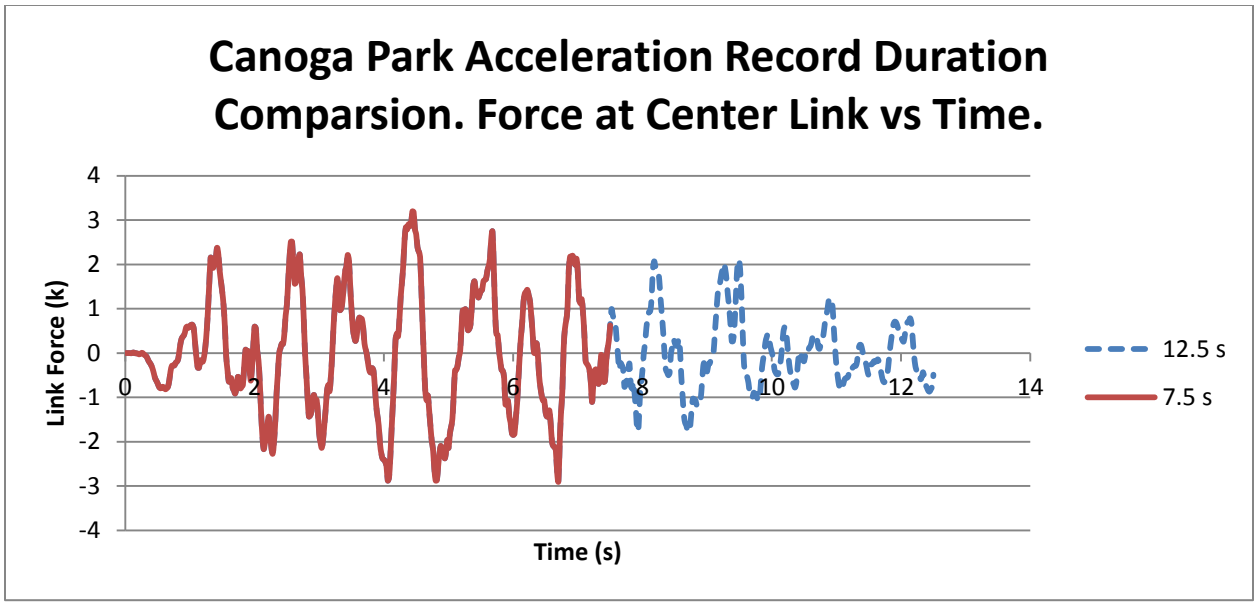

Figure 4.4 Canoga Park Acceleration Record Time Interval Data Comparison

The Tarzana Station acceleration record used was titled Tarzana – Cedar Hill Nursery A, 090. The strong motion portion of this record was clearly defined, no study of which time interval to use was needed. The full Tarzana record and the time interval used in this study are displayed in Figure 4.5.

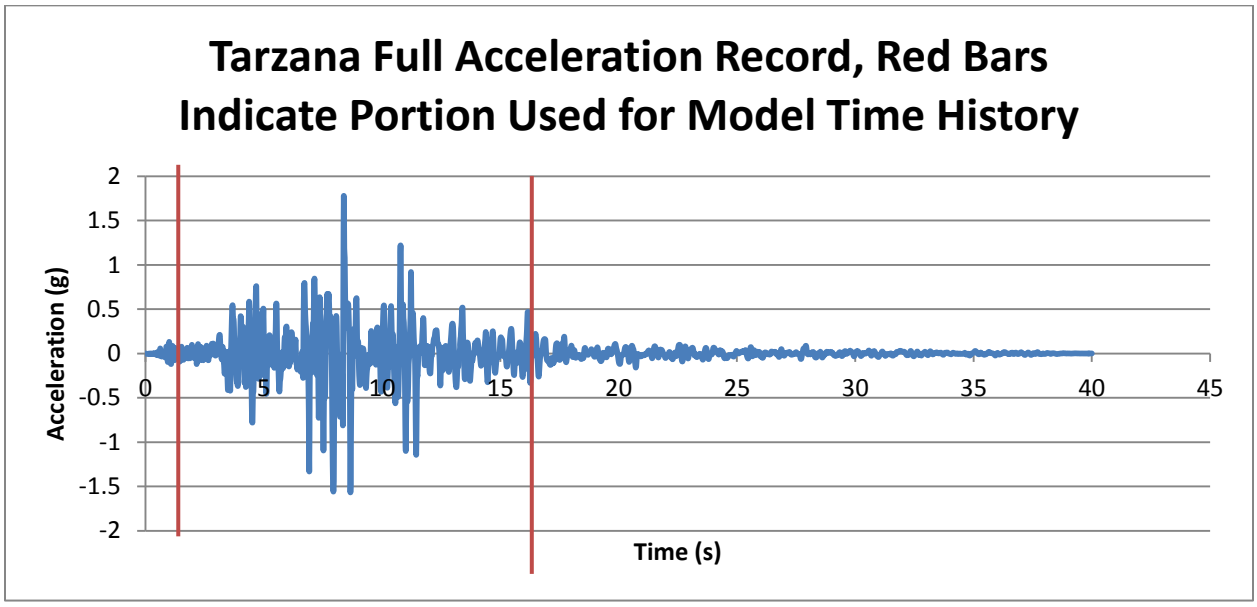

Figure 4.5 Tarzana Acceleration Record

The acceleration records described above were input into the SAP2000 program to be applied to each model as acceleration. The acceleration function used for each test was applied at the base of each model. Direct integration time history analysis was used to analyze each model. Direct integration was used because of the non-linear material properties that defined the out-of-plane wall shell elements.

4.3 Parametric Study

The parametric study consisted of 30 simulations using the models and acceleration records previously described. Data was gathered at a sample rate of 0.02 seconds to ensure accurate results. Each test and the parameters used are displayed in Table 4.3.

Table 4.3 List of Models used for the Parametric Study

Test Number	Roof Diaphragm aspect ratio	Roof Diaphragm Dimensions (ft)	Diaphragm E (ksi)	Acceleration Record
1	1:1	52 x 52	7.325	Canoga Park
2	1:1	52 x 52	14.65	Canoga Park
3	1:1	52 x 52	21.975	Canoga Park
4	1:1	52 x 52	29.3	Canoga Park
5	1:1	52 x 52	43.95	Canoga Park
6	2:1	100 x 52	7.325	Canoga Park
7	2:1	100 x 52	14.65	Canoga Park
8	2:1	100 x 52	21.975	Canoga Park
9	2:1	100 x 52	29.3	Canoga Park
10	2:1	100 x 52	43.95	Canoga Park
11	3:1	152 x 52	7.325	Canoga Park
12	3:1	152 x 52	14.65	Canoga Park
13	3:1	152 x 52	21.975	Canoga Park
14	3:1	152 x 52	29.3	Canoga Park
15	3:1	152 x 52	43.95	Canoga Park
16	4:1	200 x 52	7.325	Canoga Park
17	4:1	200 x 52	14.65	Canoga Park
18	4:1	200 x 52	21.975	Canoga Park
19	4:1	200 x 52	29.3	Canoga Park
20	4:1	200 x 52	43.95	Canoga Park
21	1:1	52 x 52	7.325	Tarzana
22	1:1	52 x 52	14.65	Tarzana
23	1:1	52 x 52	21.975	Tarzana
24	1:1	52 x 52	29.3	Tarzana
25	1:1	52 x 52	43.95	Tarzana
26	3:1	152 x 52	7.325	Tarzana
27	3:1	152 x 52	14.65	Tarzana
28	3:1	152 x 52	21.975	Tarzana
29	3:1	152 x 52	29.3	Tarzana
30	3:1	152 x 52	43.95	Tarzana

4.4 Data Collection

The focus of this study was the force transfer between the walls that were loaded out of plane and the diaphragm. The data collected consisted of nodal displacements and link force at the location of the wall/diaphragm connection. For each test, the displacement of the nodes at the wall top and the

roof edge was recorded for each time step. The displacements recorded were relative to the original displaced shape of the model. Also recorded was the force induced in each link along the entire length of the wall at each time step. SAP2000 recorded this data automatically as each simulation was completed. After each model simulation was completed, the desired data was selected and exported to spreadsheet software where it was analyzed.

5.0 Results and Analysis

This chapter discusses the results of the parametric study. Two types of data were collected, nodal displacements and link forces, each of which will be discussed separately. Throughout this chapter figures are used to demonstrate results. In each figure, a legend is used to show the stiffness of the diaphragm for each test shown. This stiffness is defined by the effective modulus of elasticity (E) of the diaphragm and represents the range of stiffness a designer might expect for steel or wood diaphragms. This method of displaying results is used for ease of comparing the effects of diaphragm stiffness on the behavior of the model.

5.1 Nodal Displacement

Nodal displacements indicated that the models behaved in the manner expected. The displacement of the node at the center of the top of the out of plane walls from each test was analyzed. An example of the deflected shape of each model is presented in

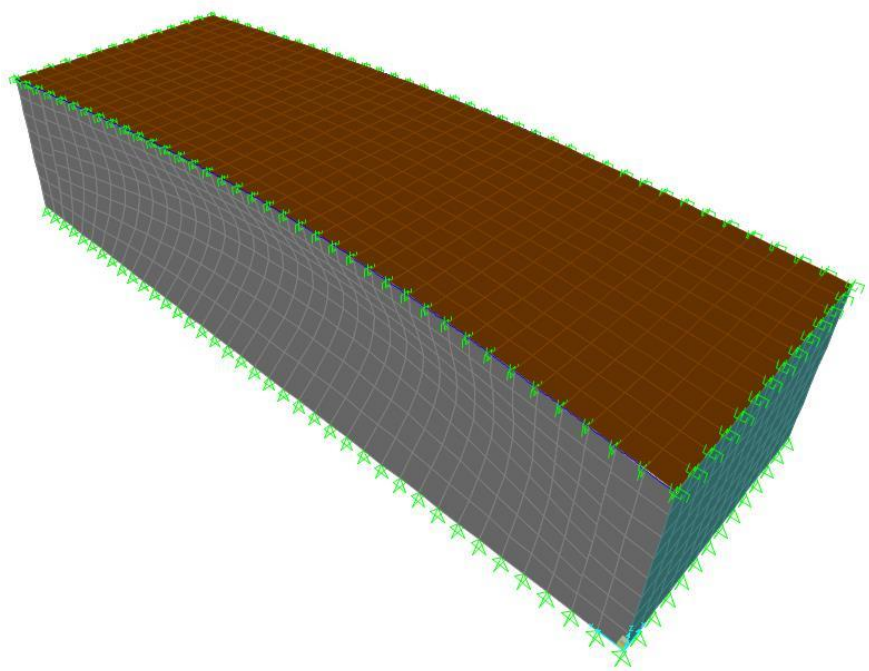

Figure 5.1 Building Model Deflected Shape Example

From discoveries of prior research, it was expected that the models would behave as a stiffness driven system, governed by diaphragm properties. By plotting the displacement vs time for each diaphragm material property tested, it became clear that the models behaved as expected. Wall node displacements during the entire duration of the acceleration record are shown for each aspect ratio in Figure 5.2 through Figure 5.7.

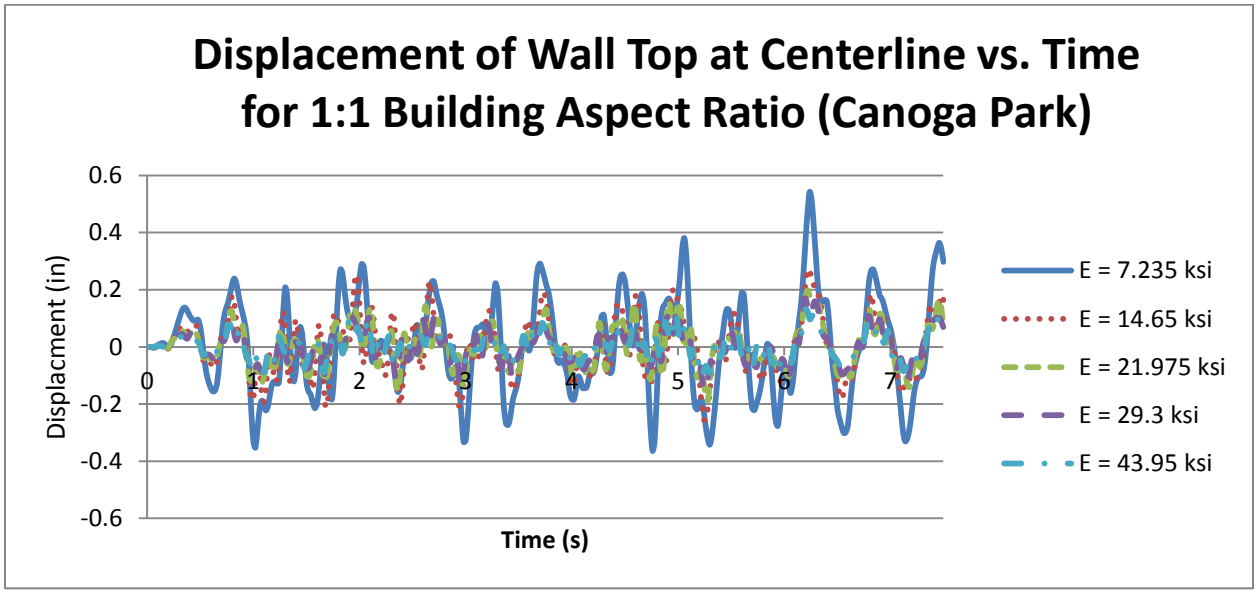

Figure 5.2 Displacement of Wall Top at Centerline for 1:1 Building Aspect Ratio (Canoga Park)

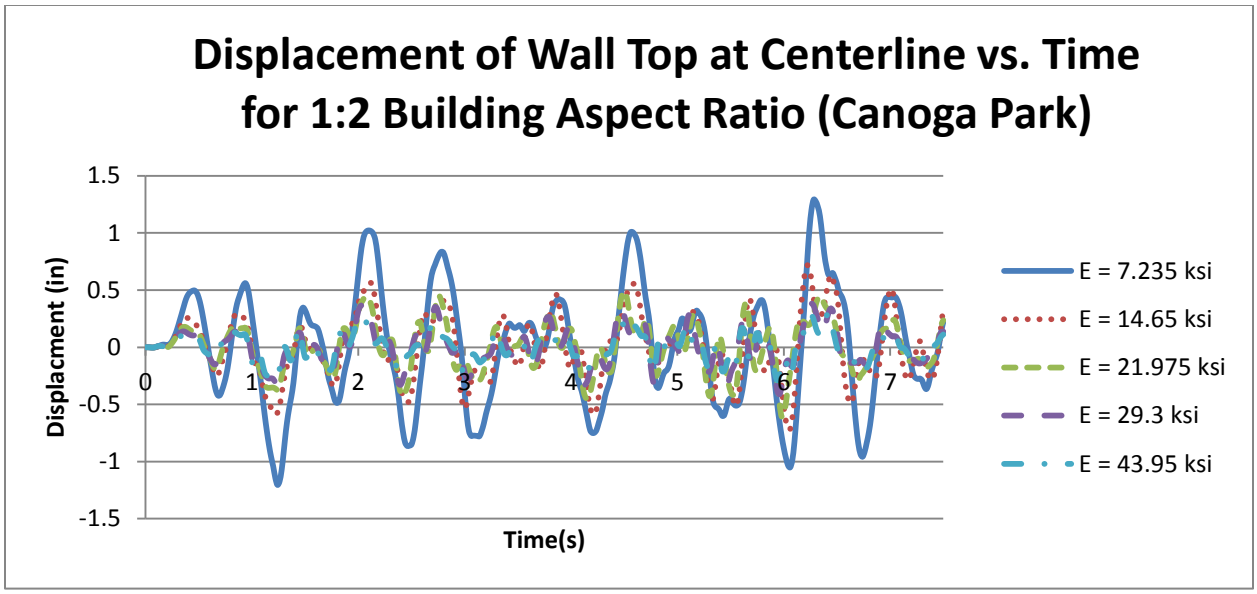

Figure 5.3 Displacement of Wall Top at Centerline for 1:2 Building Aspect Ratio (Canoga Park)

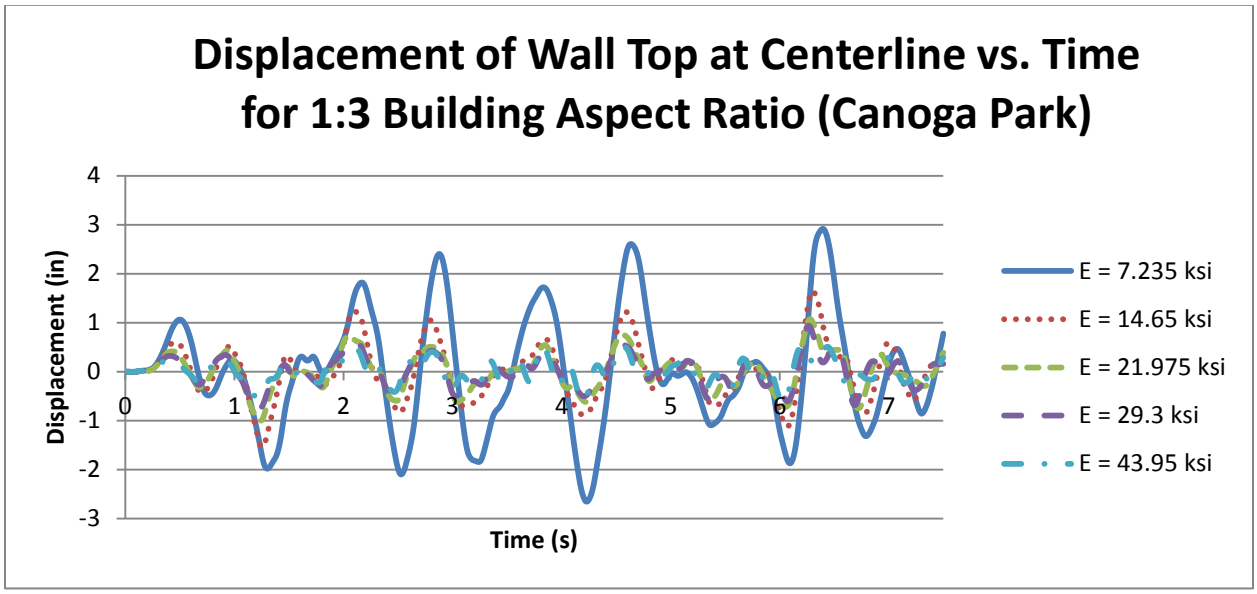

Figure 5.4 Displacement of Wall Top at Centerline for 1:3 Building Aspect Ratio (Canoga Park)

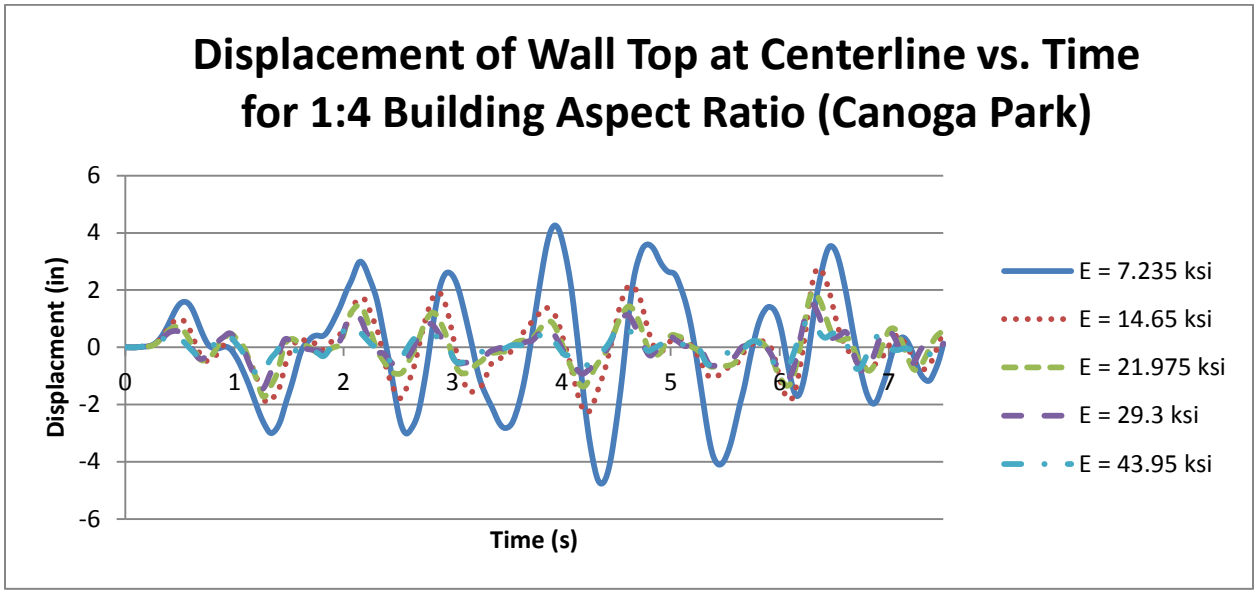

Figure 5.5 Displacement of Wall Top at Centerline for 1:4 Building Aspect Ratio (Canoga Park)

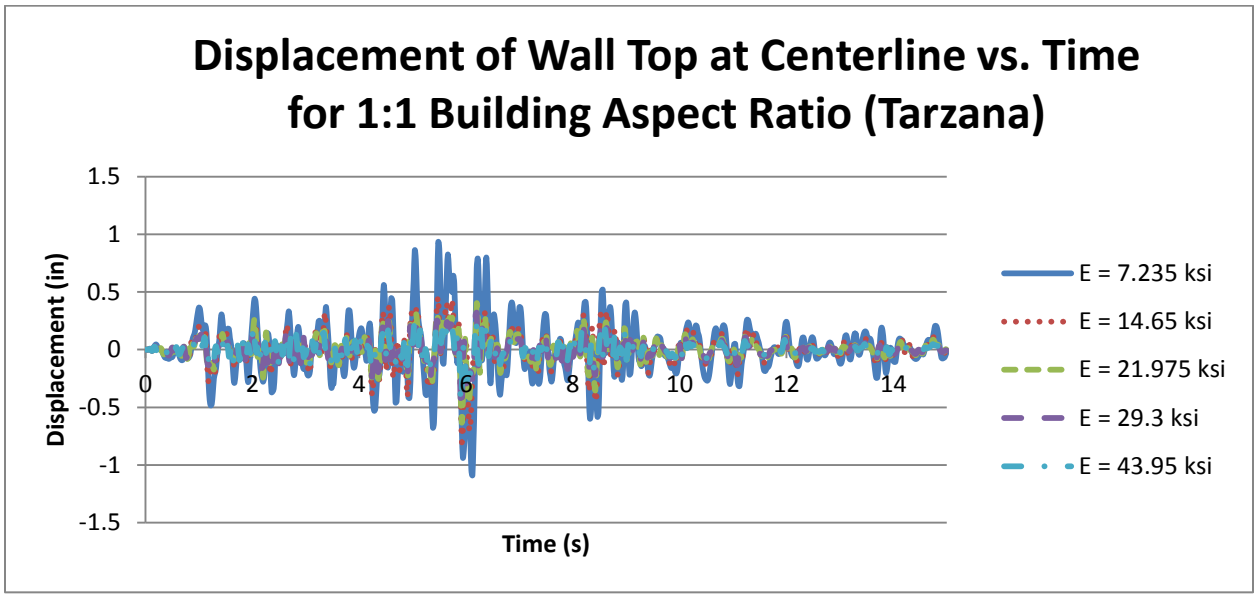

Figure 5.6 Displacement of Wall Top at Centerline for 1:1 Building Aspect Ratio, (Tarzana)

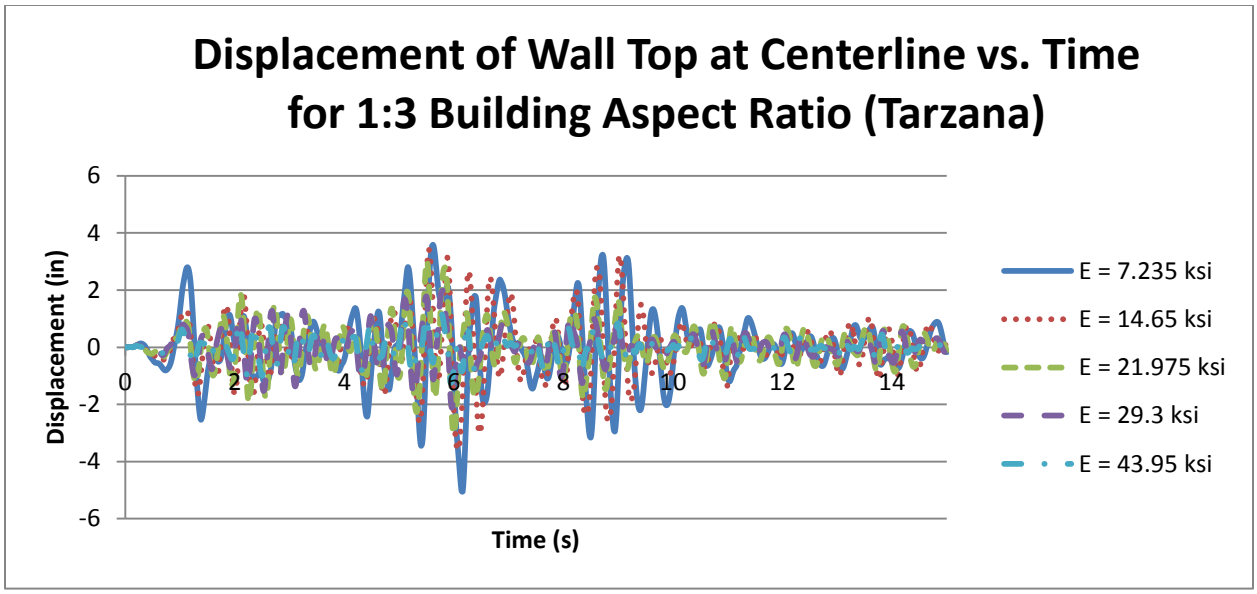

Figure 5.7 Displacement of Wall Top at Centerline for 1:3 Building Aspect Ratio (Tarzana)

From these graphs, it is clear that the models did behave like stiffness driven systems. The graphs show that within each aspect ratio the stiffest models had the smallest displacement while the most flexible had the largest displacement. The results match expected behavior and confirm that the models can be used for good comparison to the construction type being analyzed. The higher aspect ratio models had higher displacement than the lower aspect ratio models, which also match expected behavior. The highest stiffness was 6 times greater than the lowest stiffness. The maximum displacement for the 1:1 Aspect Ratio models was approximately 1 inch and for the 1:4 Aspect Ratio models was approximately 4 inches. By increasing the stiffness by a factor of 6 the displacement was reduced by approximately 75%. This change occurred in all 4 model aspect ratios.

Nodal displacements also reveal the behavior of the interaction between the wall and diaphragm. Prior research has shown that the out-of-plane walls do not contribute to the structural capacity of the lateral force resisting system, adding only additional mass to the system. From these findings it was expected that the out-of-plane walls would pull on the diaphragm in both directions of movement.

Therefore nodal displacement results were expected to show that the wall node experienced more movement than that of the roof nodes. A comparison of displacement data of the walls and diaphragm for each test model is provided in Table 5.1.

Table 5.1 Comparison of Wall and Diaphragm Displacements For Each Test

Test	Positive direction displacement (in)			Negative direction displacement (in)			Expected
	Wall	Roof	Largest	Wall	Roof	Largest	Results?
1	0.542	0.524	wall	-0.364	-0.353	wall	Yes
2	0.270	0.255	wall	-0.254	-0.241	wall	Yes
3	0.198	0.185	wall	-0.188	-0.175	wall	Yes
4	0.170	0.157	wall	-0.156	-0.143	wall	Yes
5	0.131	0.118	wall	-0.111	-0.097	wall	Yes
6	1.291	1.282	wall	-1.205	-1.191	wall	Yes
7	0.718	0.709	wall	-0.716	-0.704	wall	Yes
8	0.491	0.476	wall	-0.607	-0.592	wall	Yes
9	0.383	0.376	wall	-0.411	-0.398	wall	Yes
10	0.302	0.279	wall	-0.289	-0.278	wall	Yes
11	2.915	2.905	wall	-2.642	-2.630	wall	Yes
12	1.657	1.648	wall	-1.541	-1.526	wall	Yes
13	1.076	1.067	wall	-1.001	-0.990	wall	Yes
14	0.940	0.930	wall	-0.738	-0.726	wall	Yes
15	0.521	0.516	wall	-0.614	-0.601	wall	Yes
16	4.260	4.250	wall	-4.764	-4.750	wall	Yes
17	2.773	2.763	wall	-2.284	-2.274	wall	Yes
18	1.915	1.908	wall	-1.719	-1.706	wall	Yes
19	1.537	1.530	wall	-1.453	-1.442	wall	Yes
20	0.952	0.946	wall	-0.993	-0.983	wall	Yes
21	0.929	0.916	wall	-1.087	-1.049	wall	Yes
22	0.451	0.437	wall	-0.797	-0.769	wall	Yes
23	0.401	0.393	wall	-0.634	-0.609	wall	Yes
24	0.319	0.306	wall	-0.514	-0.481	wall	Yes
25	0.258	0.248	wall	-0.454	-0.426	wall	Yes
26	3.584	3.572	wall	-5.048	-5.027	wall	Yes
27	3.415	3.394	wall	-3.596	-3.573	wall	Yes
28	2.996	2.966	wall	-3.020	-2.999	wall	Yes
29	1.980	1.953	wall	-2.111	-2.084	wall	Yes
30	1.168	1.149	wall	-1.239	-1.222	wall	Yes

The data displayed in Table 5.1 clearly shows that the out of plane walls experience greater displacement than the roof diaphragm. This behavior confirms that the walls add additional mass to the lateral force resisting system and that the overall behavior of the models is reasonable.

5.2 Wall/Diaphragm Anchorage

This section summarizes the results of the study into the effect of the diaphragm flexibility on the force transferred by the wall/diaphragm anchorage. The results displayed in each of the following graphs are the maximum force transferred through each link at the wall diaphragm connection during the acceleration record. From these graphs, it is easy to observe the change in force transferred as the stiffness of the roof diaphragm changes. Results for the maximum force transferred by each link element throughout each test are displayed below in Figure 5.8 through Figure 5.13. Results for the simulations using *E* = 14.65 ksi in all building aspect ratios are presented in Figure 5.14. In this figure the effects of shear wall influence on the wall/diaphragm anchorage force at the edges of the diaphragm have been removed for clarity.

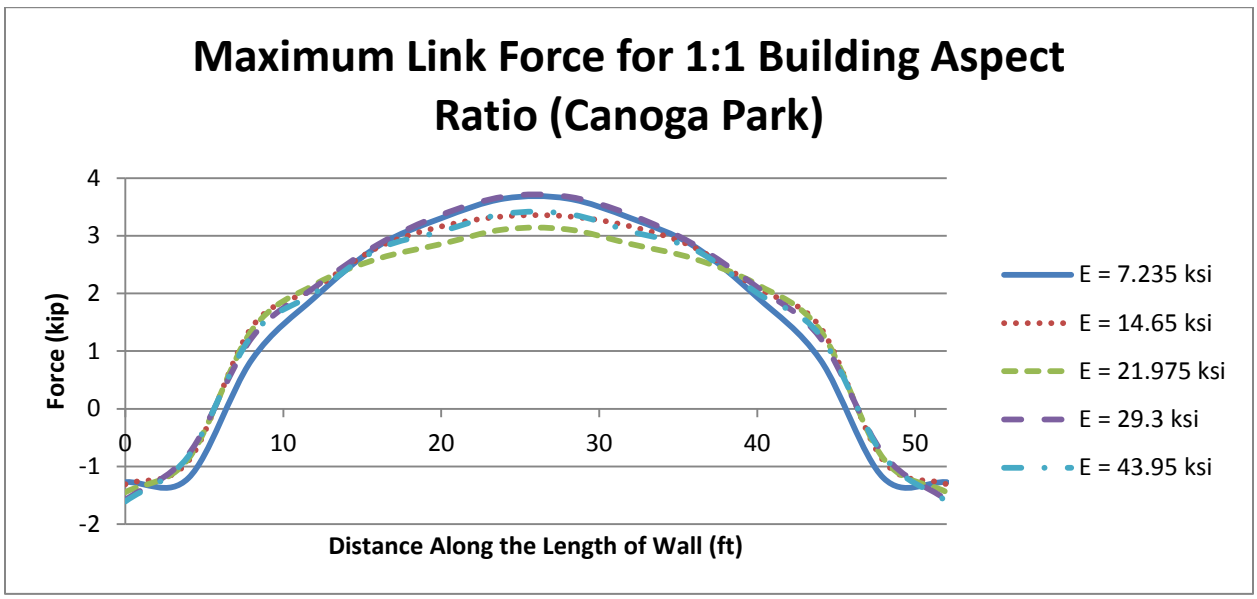

Figure 5.8 Maximum Link Forces for 1:1 Building Aspect Ratio (Canoga Park)

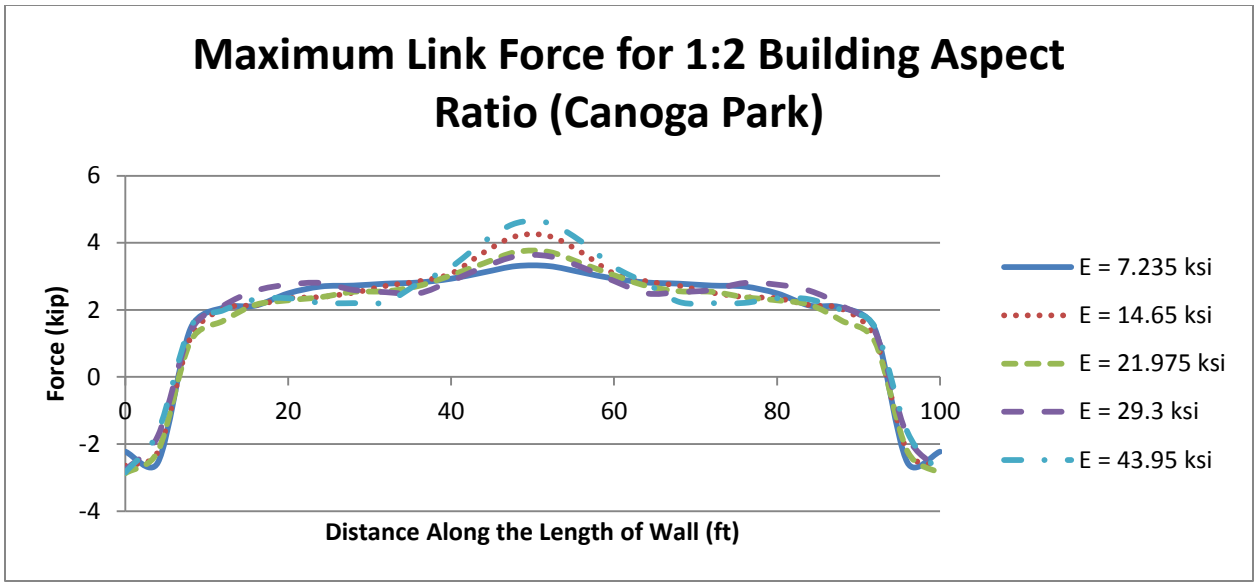

Figure 5.9 Maximum Link Forces for 1:2 Building Aspect Ratio (Canoga Park)

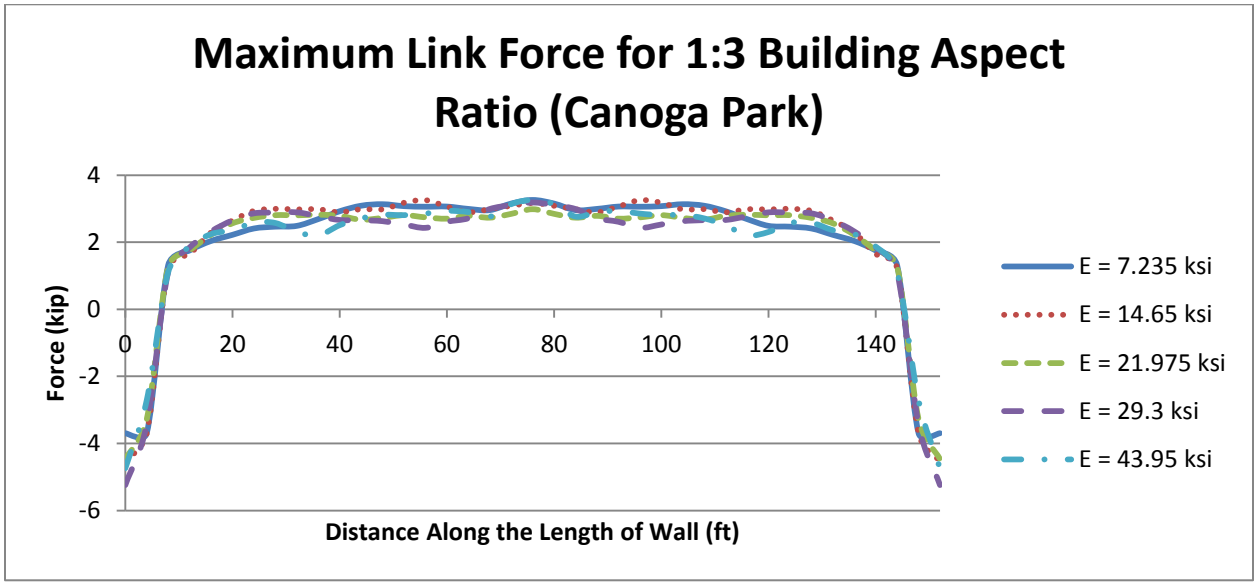

Figure 5.10 Maximum Link Forces for 1:3 Building Aspect Ratio (Canoga Park)

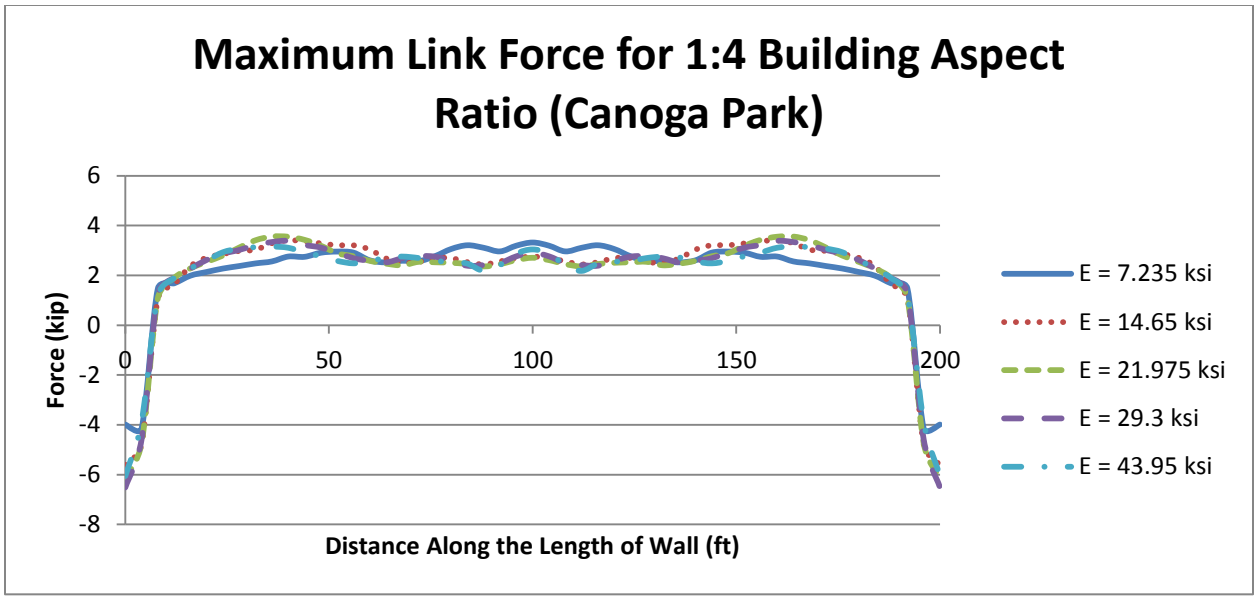

Figure 5.11 Maximum Link Forces for 1:4 Building Aspect Ratio (Canoga Park)

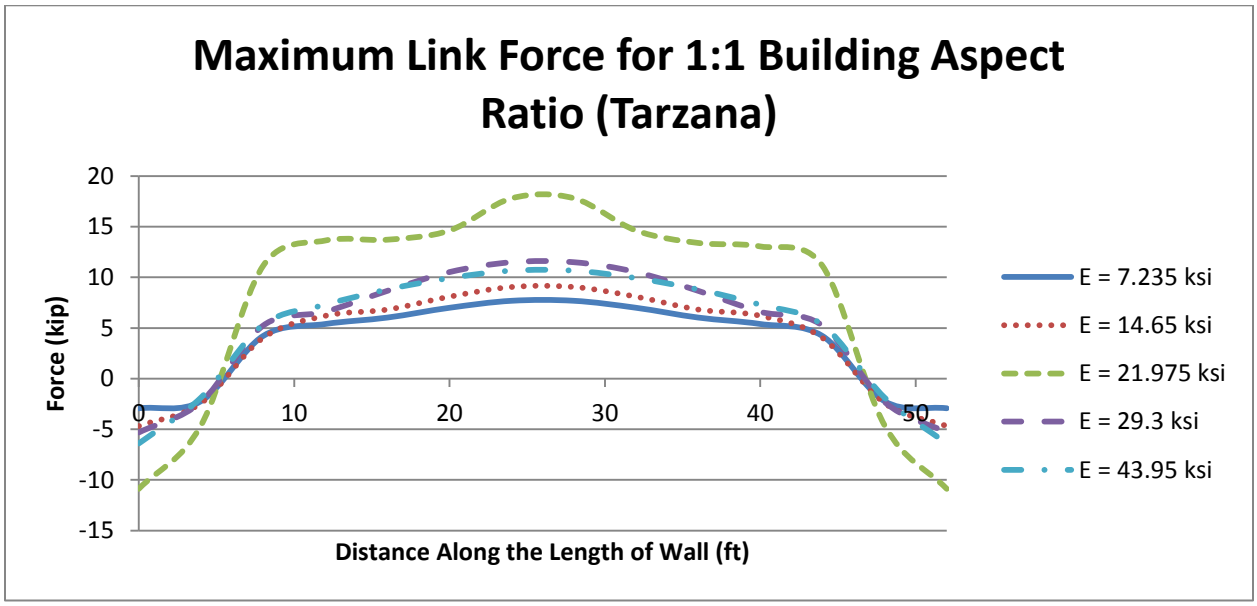

Figure 5.12 Maximum Link Forces for 1:1 Building Aspect Ratio (Tarzana)

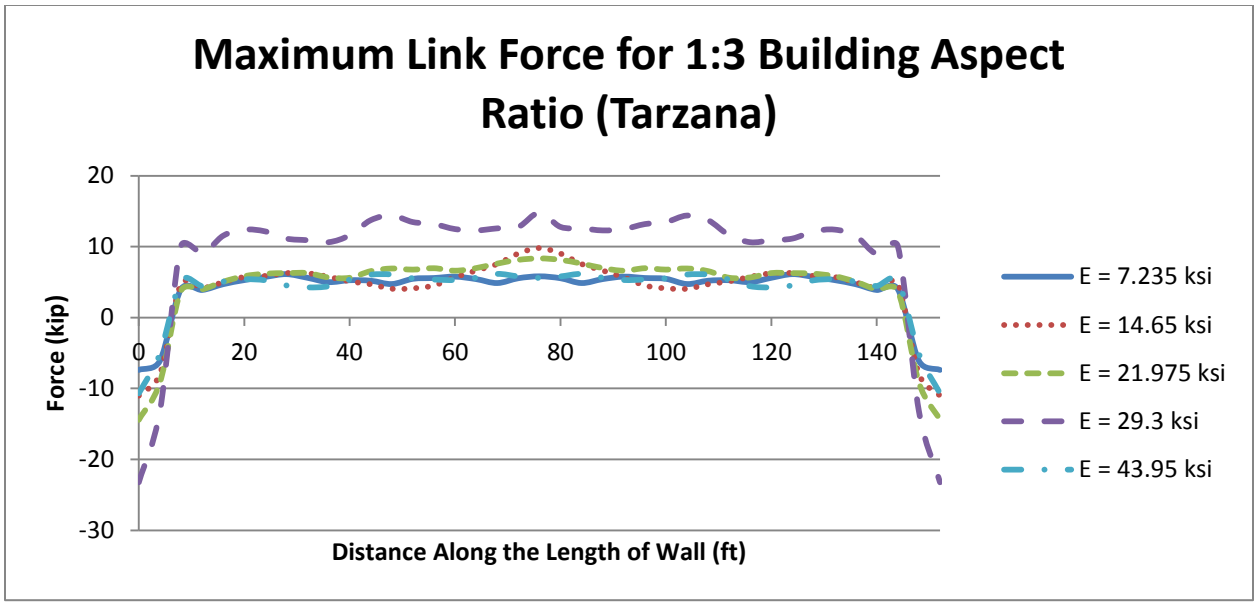

Figure 5.13 Maximum Link Forces for 1:3 Building Aspect Ratio (Tarzana)

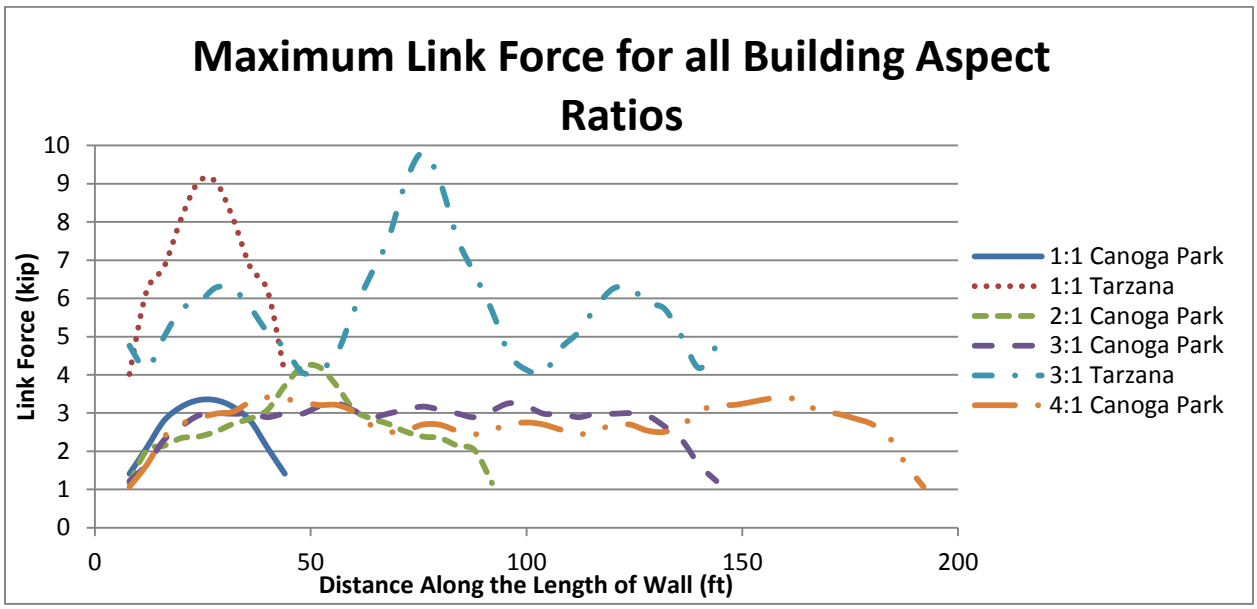

Figure 5.14 Maximum Link Forces for all Aspect Ratios

5.3 Analysis of Wall/Diaphragm Anchorage Forces

Throughout this section the trends and behavior of the test models are discussed. During the parametric study two different earthquake acceleration records were used. All references in this section

to trends in the results refer to data from both acceleration records unless otherwise specified. Results of the tests using the Canoga Park acceleration record display the same trends as results of tests using the Tarzana acceleration record. Although the trends are similar, the Tarzana acceleration record contained much larger accelerations, resulting in higher displacements and forces than tests using the Canoga Park record. The Tarzana earthquake record contains peak ground accelerations as large as that of the maximum considered earthquake for structural design. Higher than expected link forces were recorded in Test Numbers 23 and 29, which are shown in Figure 5.12 and Figure 5.13 respectively. This was due to resonance that occurred in each of those simulations.

Discussion about the behavior of the models is necessary to understand data displayed in each of the previous figures. The use of Rayleigh Damping to reduce the effect of higher order mode shapes did not completely remove their influence. The higher order mode shapes had negligible effect on the smaller aspect ratio models, but were present in the 1:3 and 1:4 aspect ratio models. The higher order mode shapes were more prevalent in the larger aspect ratio models because the longer wall length allowed for the mode shapes to be more influential. The effect of these mode shapes was to distort the smooth distribution of the maximum force transferred by each link. This behavior is not noticeable in the 1:1 and 1:2 aspect ratio simulations but is present in the 1:3 and 1:4 aspect ratio simulations. An additional effect of this behavior was the distortion of the relationship between diaphragm stiffness and force transferred by the link. The data displayed in each of the previous figures show no discernible relationship between diaphragm stiffness and link force. Due to this behavior, discussion of the data will be limited to the envelope of forces observed.

The results of each test show that the diaphragm acts as a beam on an elastic foundation due to the out-of-plane walls providing continuous support. To gain greater understanding of this behavior refer to Hetenyi (1946). This behavior is important to recognize in order to understand the shape of the

distribution of forces. Loads applied to beams on elastic foundations decay over a length called the decay length along the axis of the beam. This decay length is dependent on the stiffness of the supporting medium. For this study the supporting medium was the out-of-plane wall elements. This behavior drives the shape of the distributed force graphs.

Results show that in the 1:1 aspect ratio models the decay length of the load applied on the diaphragm by the weight of the masonry walls causes a parabolic distribution of forces in the link elements. Models of the 1:3 and 1:4 aspect ratio buildings do not have a parabolic distribution of forces. This is because the decay length effect is nullified by the large number of link elements across the length of the wall and the parabolic distributions of force associated with each link are masked by the superposition of the force distribution associated with the adjacent connections. Results of the 1:2 aspect ratio tests show a transition in the link force distribution from that of the 1:1 to the distributions of the 1:3 and 1:4 aspect ratio buildings. From these results it can be concluded that in high aspect ratio buildings each anchor bolt transfers very similar forces, while in low aspect ratio buildings the forces transferred at the center of the diaphragm are highest.

The relatively close spacing of the results for each of the 5 diaphragm stiffness properties tested for a given aspect ratio suggest that the link force is not heavily influenced by diaphragm stiffness. This was contrary to what was initially expected. The diaphragm stiffness properties tested were selected to cover a range of diaphragms used in common construction practices. Due to this, it can be concluded that the range of forces recorded in this study reflect feasible values that can occur in structures during seismic events.

Currently, wall to diaphragm anchorage is designed in terms of force distributed to each bolt by tributary area. In order to compare the results of this study to current design practices, data on the force at each bolt was used to generate graphs showing the distribution of forces across the length of a

diaphragm. The maximum force transferred by each link during all 5 different stiffness tests for a given aspect ratio and acceleration record was used to compute the distributed force. Each link was spaced at 4 feet; this length was used to compute the distributed force. Data for the maximum force transferred between the wall and diaphragm for each aspect ratio tested are displayed below in Figure 5.15 through Figure 5.20.

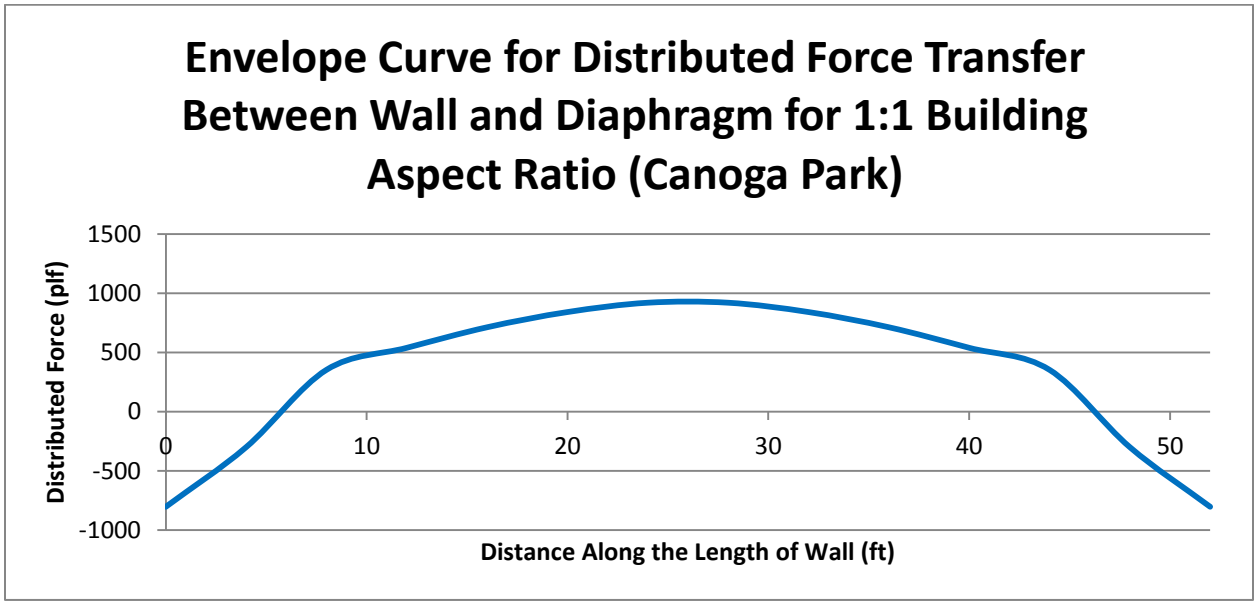

Figure 5.15 Wall/Diaphragm Force Transfer for 1:1 Building Aspect Ratio (Canoga Park)

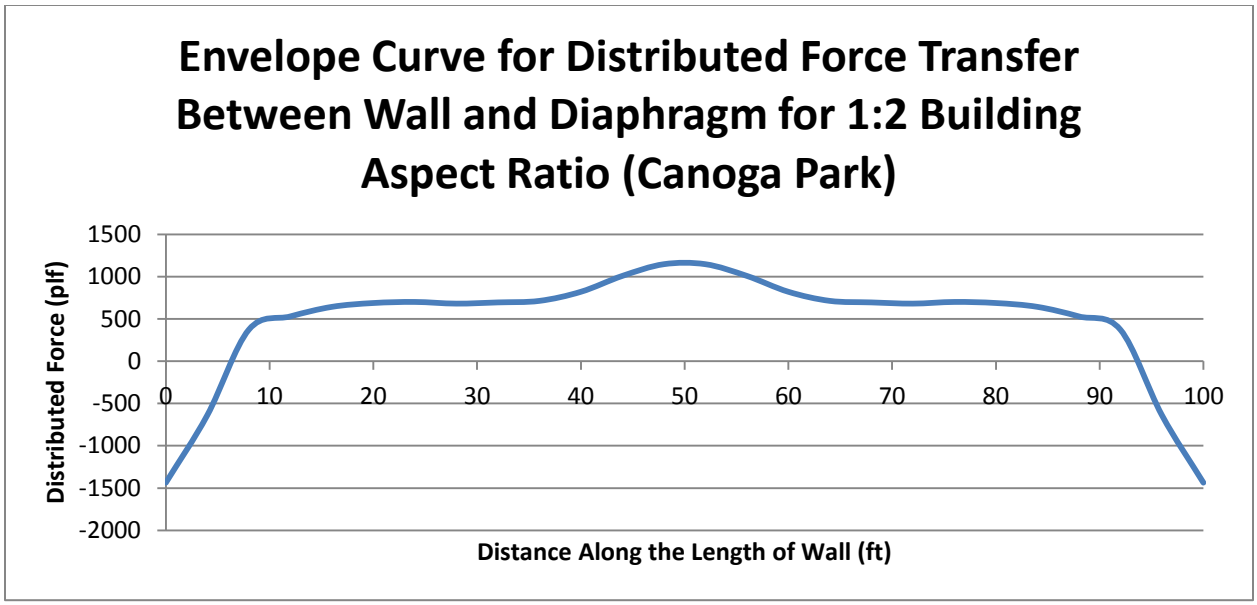

Figure 5.16 Wall/Diaphragm Force Transfer for 1:2 Building Aspect Ratio (Canoga Park)

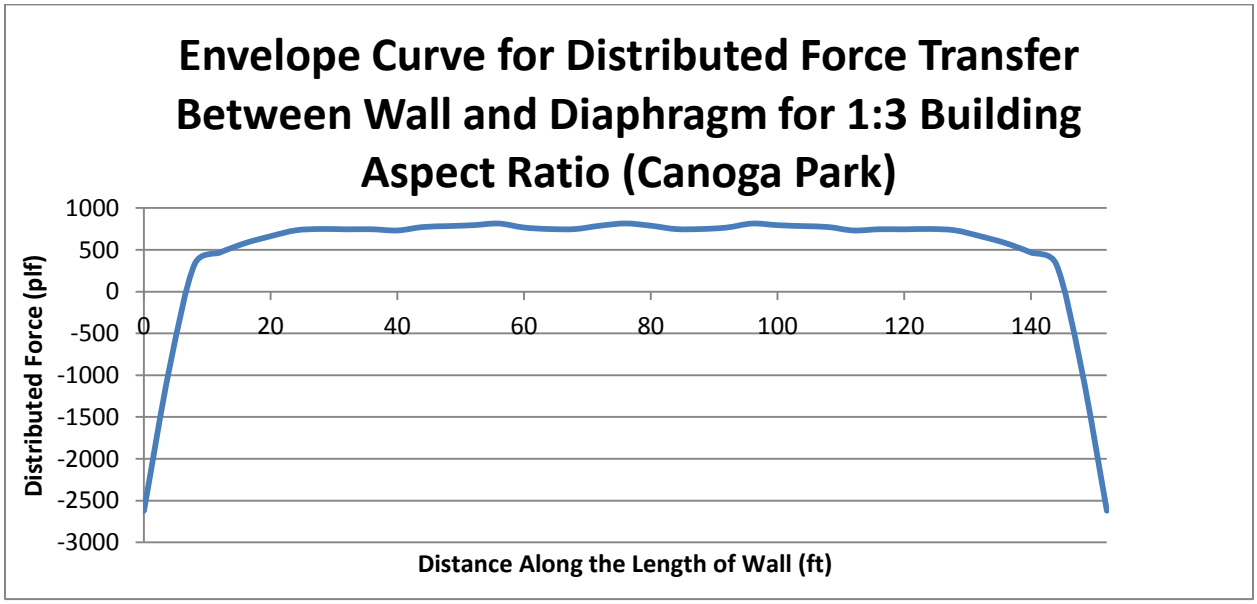

Figure 5.17 Wall/Diaphragm Force Transfer for 1:3 Building Aspect Ratio (Canoga Park)

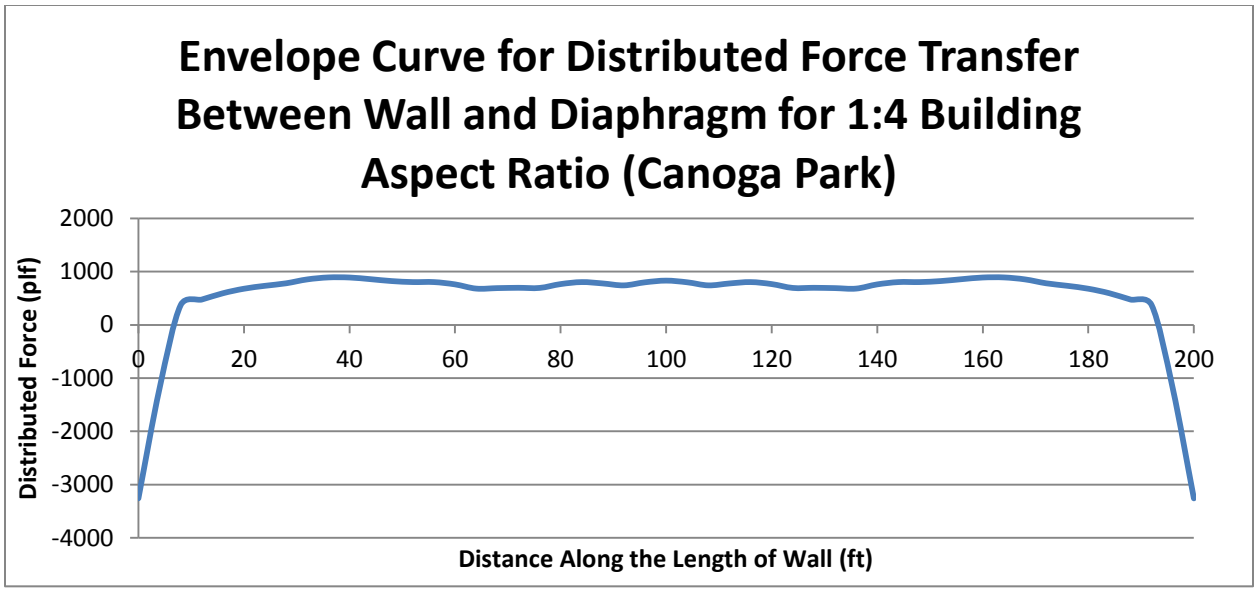

Figure 5.18 Wall/Diaphragm Force Transfer for 1:4 Building Aspect Ratio (Canoga Park)

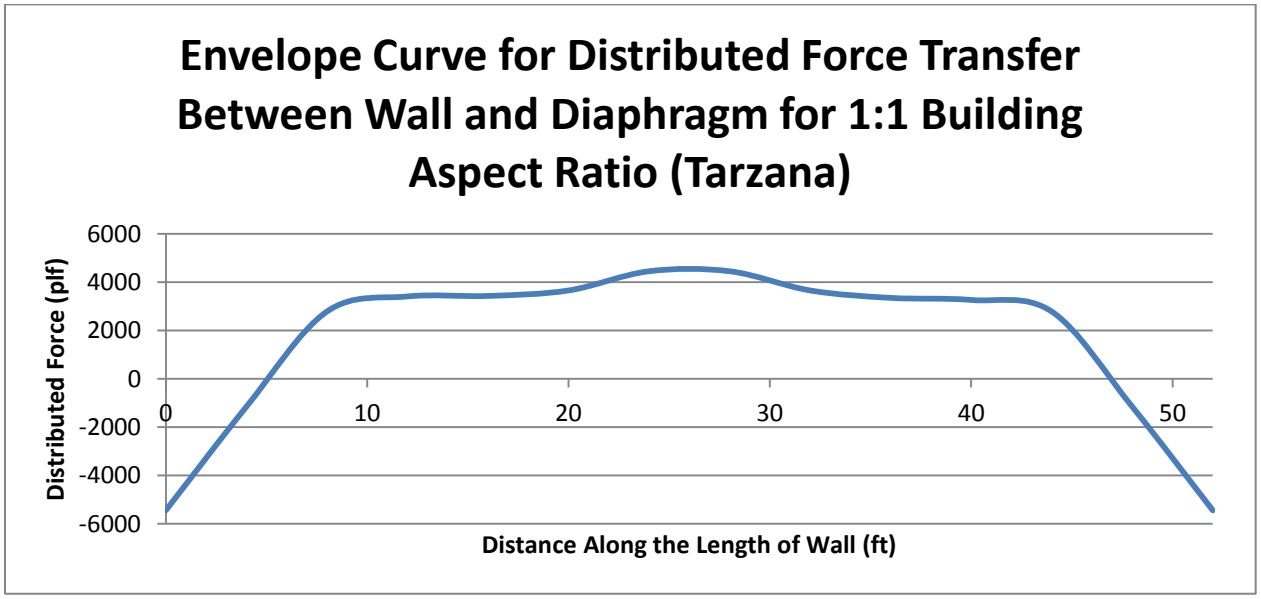

Figure 5.19 Wall/Diaphragm Force Transfer for 1:1 Building Aspect Ratio (Tarzana)

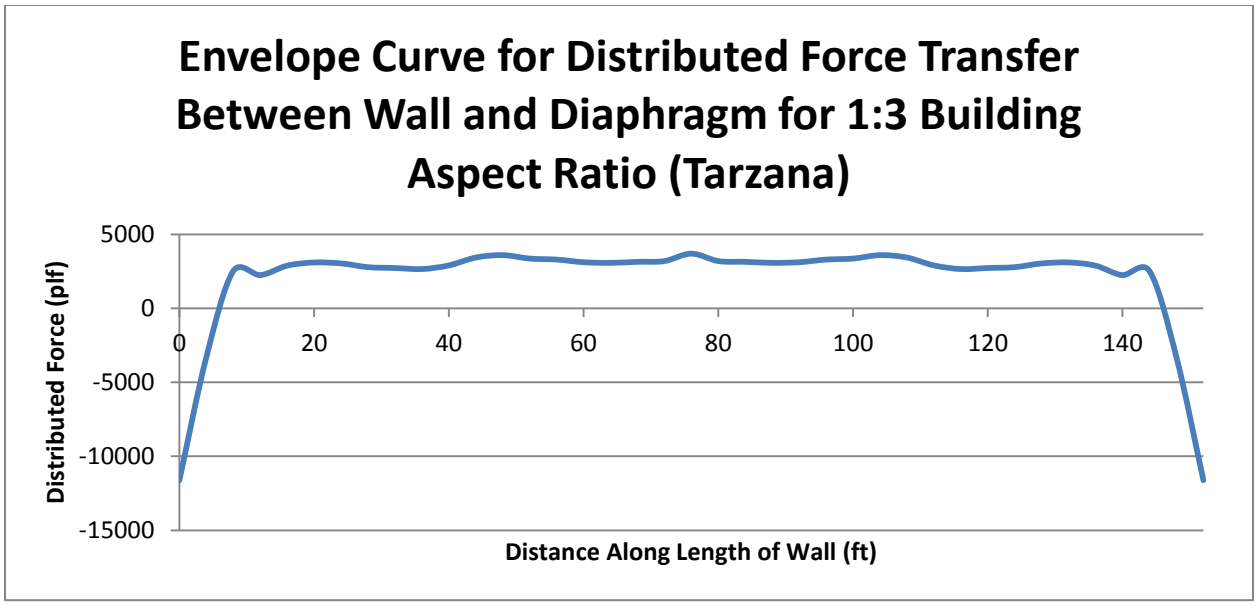

Figure 5.20 Wall/Diaphragm Force Transfer for 1:3 Building Aspect Ratio (Tarzana)

Data shown in the previous graphs can be used to understand the force transferred at the wall diaphragm interface. The maximum force transferred for each simulation using the Canoga Park acceleration record was approximately 800 pounds per lineal foot (plf). Forces of about 1200 plf occurred in the 1:2 building aspect ratio simulations. This was due to higher order mode shapes causing larger forces to be transferred through the link elements near the center of the diaphragms. The data for the 1:2 aspect ratio simulations shows that these forces are not indicative of the force transferred through link elements throughout the rest of the diaphragm. The average force transferred for each simulation using the Tarzana acceleration record was approximately 3700 plf. The negative force values transferred at the end of each data line should be disregarded as this is due to effects of the interaction with the shear walls. The force transferred in the interior portions of the building is solely due to the weight of the walls being loaded in the out-of-plane direction and pulling/pushing on the diaphragm. This is because diaphragm stiffness does not have a significant impact on the force transferred as

previously discussed in this section. A comparison of the envelope curves from Figure 5.15 to Figure 5.20 is presented in Figure 5.21. In this figure the effects of shear wall influence on the wall/diaphragm anchorage force at the edges of the diaphragm have been removed for clarity.

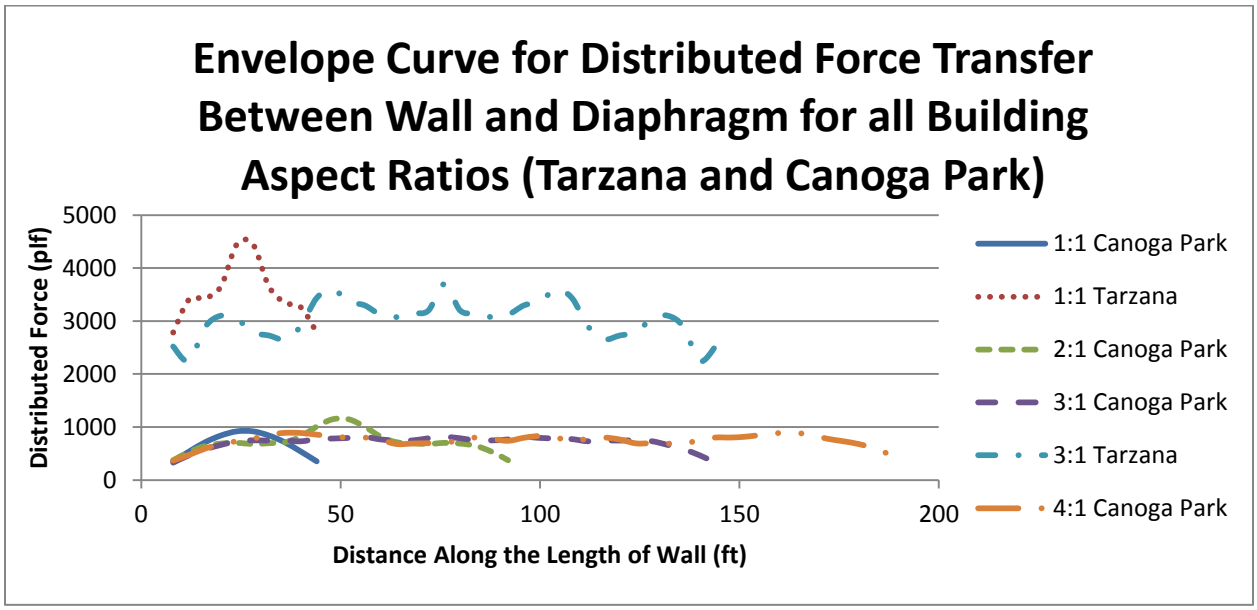

Figure 5.21 Wall/Diaphragm Force Transfer for all Building Aspect Ratios

The results show that the current design standards do not fully consider the force transferred by the wall and diaphragm. Current design standards require anchorage to be designed to a lower capacity than the demand observed in this study. The capacity for 1-inch anchor bolts, spaced 4 feet apart, as determined using section 3.1.6.3.2 of the MSJC (2011) is 2829 lb or 708 plf. The calculation for bolt capacity is shown in the appendix. This capacity is shown to be insufficient by the results of this study, as it is only 19% of the maximum force recorded. As discussed in the introduction to this study, the current solution to this disparity between anchorage capacity and demand is the use of continuous lateral ties. The ties transfer the anchorage force deep into the diaphragm and into the opposing wall. This approach is not efficient and does not address the issue of the lack of capacity at the wall diaphragm interface.

To compare the Tarzana and Canoga Park acceleration records to design standards the design level acceleration and maximum considered acceleration are used. For both locations (Tarzana and Canoga Park) the design level earthquake motion (S_{DS}) is 1.0g and the maximum considered earthquake motion (S_{MS}) is 1.5g. These values were calculated using procedures in ASCE §12.8 (2010). The Canoga Park acceleration record contains smaller accelerations than the S_{DS} in that location. The Tarzana acceleration record contains accelerations higher than the S_{MS} in that location. This is the ground acceleration used to compute the lateral loads on a structure in these locations. The peak ground acceleration (PGA) in the Tarzana record was 1.7g. This shows that loads similar to the loads recorded during the simulations can be generated from the PGA used in the ASCE (ASCE7-10 §12.8) to design lateral force resisting systems.

The results of this study have implications on the design of subdiaphragms, which are currently used to mitigate the construction cost of continuous lateral ties. Using continuous lateral ties is very expensive because at all girder/joist connections must be capable of transferring the wall anchorage force. Subdiaphragms reduce the amount of these splice connections necessary in each diaphragm. If new standards on the design of the wall/diaphragm connection were developed, the need for continuous splice connections may be eliminated. This would lead to a simpler diaphragm design and construction process.

The ultimate goal of this study was to determine the effect of the stiffness of roof diaphragms on the wall diaphragm anchorage force. For a practical range of diaphragm stiffness properties the anchorage force was relatively unchanged. From the results of this study, it is shown that the force transferred at the wall/diaphragm interface is greater than what is currently required by the building code.

6.0 Conclusions

The stated goal of this study was to investigate the effects of diaphragm stiffness on the force transferred at the wall/diaphragm interface in low-rise masonry construction. In order to complete this study several steps were taken. Initially, a review of previous studies published on the behavior of low-rise masonry buildings was completed. This research included material covering studies of practical test models of walls, diaphragms and scaled buildings. Also included in the research prior to this study was an investigation of developments into the use of finite element analysis to model these types of structures. Once the overview was complete, the initial stages of this study were started. A building model was developed using the finite element software, SAP2000. Each portion of the model was verified against practical test data to ensure the model produced accurate results. Once the model was completed, it was used to test 30 different aspect ratio and diaphragm stiffness configurations loaded with an earthquake acceleration record. Data from these tests was then used to generate results and conclusions about the effects of diaphragm stiffness on wall/diaphragm anchorage forces.

From this study several conclusions were made about the wall/diaphragm anchorage forces in low-rise masonry structures.

1: The effect of diaphragm stiffness on anchorage forces in low-rise masonry buildings is not significant for a reasonable range of diaphragm stiffness properties. In order to produce a significant change in the wall/diaphragm connection force by changing the diaphragm stiffness an unrealistic stiffness would have to be used. This means that the force transferred at the connection is only affected by the stiffness of the connection itself.

2: The aspect ratio of the roof diaphragm has a minimal effect on the force transferred at the wall/diaphragm connection. For all aspect ratios tested the anchorage force remained relatively constant at 800 plf in the Canoga Park simulations and 3700 plf in the Tarzana simulations.

3: The aspect ratio of the roof diaphragm changes the distribution of force transferred at the wall/diaphragm connection. In low diaphragm aspect ratio buildings, the forces transferred are distributed in a parabolic shape across the length of walls perpendicular to the direction of loading. This means that higher forces are transferred in the center of the diaphragm than in areas closer to the shear walls. In higher aspect ratio buildings, the forces transferred are evenly distributed and their magnitude is that of the peak of the parabolic shape that describes the force transferred in low aspect ratio buildings.

4: Current design standards for the capacity of the wall/diaphragm anchorage do not meet the demand of this type of connection. This study has shown that current standards only meet 19% of the shear force demand on each anchor bolt. As previously mentioned, the current solution for this is to use continuous lateral ties.

The above conclusions can be inferred from simulations run by this study, but it is important to understand the limitations of the models used. Each model was calibrated to correctly respond to motion in one direction only. This is a simplification, as seismic events do not behave in this manner. During a seismic event, shaking would occur in multiple directions, inducing torsion in a building. The link element used to transfer force was only capable of resisting shear. Axial stiffness was not considered. These limitations were assumed to have minimal impact on the results of this study because the models were shown to be accurate in producing the behavior of interest.

Further research into this subject should involve practical testing to investigate the feasibility of a connection that can resist the forces transferred at the wall/diaphragm interface. The current standard of ties across the depth of a diaphragm might possibly become obsolete with a new connection design. A new connection might be more economical than the use of continuous ties as these ties require continuity connections throughout the diaphragm.

Additional implications of this study are possible building code changes that would consider the parabolic shape of the force transferred between the wall and diaphragm for lower aspect ratios. Currently, each anchor bolt is designed to have the same capacity across the entire length of the wall. By allowing the connection to have a lower capacity at the edges of the diaphragm than in the center, a more economical design can be achieved.

Bibliography

American Forest & Paper Association (AF&PA), (2005). National Design Specification for Wood Construction, 2005 Edition, AF&PA. Washington, DC.

American Society of Civil Engineers (ASCE), (2010). *Minimum Design Loads for Buildings and Other Structure, 2010 Edition,* ASCE. Reston, VA.

Bott, J. W. (2004). "Horizontal Stiffness of Wood Diaphragms." M.S. Thesis, Virginia Polytechnic Institute and State University, Blacksburg, VA.

Brown, R. H., and Whitlock, A. R. (1983). "Strength of Anchor Bolts in Grouted Concrete Masonry." *Journal of Strucutral Engineering,* 109(6), 1362-1374.

Bruneau, M. (1995). "Performance of Masonry Structures During the 1994 Northridge (Los Angeles) Earthquake." *Canadian Journal of Civil Engineering, 22*:378-402.

Cohen, G. L. (2001). *Seismic Response of Low-rise Masonry Buildings With Flexibile Roof Diaphragms*. MS Thesis, The Univserity of Texas at Austin, Austin, TX.

Cohen, G. L. (2004). *Seismic Evaluations and Rehabilitaion of Low-Rise Reinforced Masonry Buildings with Flexible Diaphragms*. Ph.D. Dissertation, The University of Texas at Austin, Austin, TX.

Costley, A. P., and Abrams, D. A. (1995). "Dynamic Response of Unreinforced Masonry Buildings With Flexibile Diaphragms." *Department of Civil Engingeering University of Illinois at Urbana-Champaign*, Urbana, IL.

Duncan, R. and J. D. Dolan. (2012). *Floor Diaphragm Testing Utilizing Engineered I-Joist Framing and 19/32-Inch OSB Sheathing in 24 Foot Dimensions*. Report No. CMEC 11-020-2 prepared for ITW Paslode, Vernon Hills, IL.

Countryman, D. (1952). Lateral Tests on Plywood Sheathed Diaphragms. Douglas Fir Plywood Association Laboratory Report Number 55, Tacoma, WA.

Ekwueme, C., (2005). "Anchorage of Concrete Masonry Walls." *Masonry Chronicles*, Winter 2005-06.

Essa, H. S., Tremblay, R., and Rogers, C. A. (2003). "Behavior of Roof Deck Diaphragms Under Quasistatic Cyclic Loading." *Journal of Structural Engineering,* 129(12), 1658-1666.

Falk, R. H., and Itani, R. Y. (1989). "Finite Element Modeling of Wood Diaphragms." *Journal of Strucutral Engineering,* 115(3), 543-559.

Hatzinikolas, M. A., Lee, R., Longworth, J., and Warwuck, J. (1983). *Structural Engineering Report No. 111 Drilled-in Inserts in Masonry Construction*. The Univserity of Alberta, Edmondton, AB.

He, M., and Li, Z. (2012). "Lateral Performance of Light Wood Diaphragms with Different Structural Configurations Under Monotonic Load." *Advanced Materials Research,* Vols. 368-373, 349-352.

Hetenyi, M. (1946). *Beams on Elastic Foundation*, The University of Michigan Press, Ann Arbor, MI.

International Code Council (ICC), (2012). *International Building Code*. International Code Council Inc., Whittier, CA.

Itani, R. Y., and Cheung, C. K. (1984). "Nonlinear Analysis of Sheathed." *Journal of Structural Engineering,* 110(9), 2137-2147.

Jo, S. (2010). *Seismic Behavior and Design of Low-rise Reinforced Concrete Masonry with Clay Masonry Veneer*. P.h. D. Dissertation, The University of Texas at Austin, Austin, TX.

Judd, J. P., and Fonseca, F. S. (2005). "Anayltical Model for Sheathing-to-Framing Connections in Wood Shear Walls and Diaphragm." *Journal of Structural Engineering,* 131(2), 345-352.

Karim, A. A., Quenneville, P., Sa'don, N. M., and Ingham, J. M. (2011). "Wall-Diaphragm Connection Assessment Guidelines for URM Buildings." *Proceedings of the Ninth Pacific Conference on Earthquake Engineering: Building an Earthquake-Resilient Society*, NZSEE, Auckland, New Zealand

Klinger, R. E., McLean, D. I., McGinley, M. W., Shing, P. B., Seongwoo, J., and Okail, H. (2010). *Performance-based Design of Masonry and Masonry Veneer.* National Science Foundation, Austin, TX, Pullman, WA, San Deigo, CA.

Lawson, J. W., and Yarber, C. N. (2013). "Collective Chord Behavior in Large Flexible Diaphragms." *Proceedings of the ASCE Structures Congress 2013,* ASCE. Reston, VA

Lin, T.-J., and LaFave, J. M. (2012). "Experimental Structural Behavior of Wall-Diaphragm Connections for Older Masonry Buildings." *Construction and Building Materals,* 26:180-189.

Luttrell, L. D. (1967). "Strength and Behavior of Light-gage Steel Shear Diaphragms." *Cornell Engineering Research Bulletin,* 67-1.

Masonry Standards Joint Committee (MSJC). (2011). *Building Code Requirements and Specification for Masonry Structures*, 2011 Edition, The Masonry Society. Boulder, CO.

Pant, S. (2013). *Numerical Study of the Structural Performance of Large Panelized All-wood Roof Diaphragms*. M.S. Thesis. Clemson University. Clemson, SC.

Pacific Earthquake Engineering Research Center (PEER). "PEER Ground Motion Database." *PEER.* <http://peer.berkeley.edu/products/strong_ground_motion_db.html> (Dec. 13, 2013).

Peterson, J. (1983). "Bibliography on Lumber and Wood Panel Diaphragm." *Journal of Structural Engineering,* 109(12), 2838-2852.

Rogers, C. A., and Tremblay, R. (2003). "Inelastic Seismic Response of Frame Fasteners for Steel Roof Deck Diaphragms." *Journal of Structural Engineering,* 129(12), 1647-1657.

Shedid, M. T., El-Dakhakhni, W. W., and Drysdale, R. G. (2009). "Beavior of Fully Grouted Reinforced Concrete Masonry Shear Walls Failing in Flexure: Analysis." *Engineering Structures,* 31:2032-2044.

Skaggs, T. D., and Martin, Z. A. (2004). "Estimating Wood Structural Panel Diaphragm and Shear Wall Deflection." *Practical Periodical on Structural Design and Construction,* 9(3), 136-141.

Tena-Colunga, A. (1992). "Seismic Evaluation of Unreinforced Masonry Structures with Flexibile Diaphragms." *Earthquake Spectra,* 8(2), 305-318.

Tena-Colunga, A., and Abrams, D. P. (1996). "Seismic Behavior of Structures With Flexible Diaphragms." *Journal of Structural Engineering,* 122(4), 439-445.

Tissell, J. R., and Elliott, J. R. (2004). *"Report 138: Plywood Diaphragms."* APA The Engineered Wood Association Report 138, Tacoma, WA.

Ueda, T., Kitipornchai, S., and Ling, K. (1990). "Experimental Investigation of Anchor Bolts Under Shear." *Journal of Structrual Engineering,* 116(4), 910-921.

Weigel, T. A., Mohsen, J. P., Burke, A., Erdmann, K., and Schad, A. (2002). "Tensile Strength of Headed Anchor Bolts in Tops of Fully Grouted Concrete Masonry Walls." *TMS Journal.* The Masonry Society. Bolder, CO

Yarber, C. N. (2012, August). *Experimental Determination of the Stiffness and Strength of Continuity Tie Connections in Large Wood Roof Diapharagms and Impact on the Collective Chord Model*. MS Thesis. California Polytechnic State University, San Luis Obispo, CA.

Yi, T. (2004). *Experimental Investigation and Numerical Simulation of an Unfreinforced Masonry Structure with Flexibile Diaphragms*. P.h. D. Dissertation. Georgia Institue of Technology, Atlanta, GA.

Appendix

Anchor Bolt Shear Capacity

The bolt shear capacity used in the results and analysis section of this thesis was calculated using the following procedure:

MSJC §3.1.6.3.2 defines bolt shear capacity as the minimum of the following:

$Bvnb = 4*Apv*(f'm)^{.5}$ eq. 3-6

$Bvnc = 1050*(f'm*Ab)^{.25}$ eq. 3-7

$Bvnpry = 8*Apt*(f'm)^{.5}$ eq. 3-8

$Bvns = 0.6AbFy$ eq. 3-9

Apv = projected area for shear

$Apv = .5*\prod*Lbe^2$ eq. 1-5

Lbe = bolt edge distance

Lbe = (7 5/8)*.5 = 3.8125 "

$Apv = .5*\prod*(3.8125)^2$

$Apv = 22.83\ in^2$

Ab = cross sectional area of the bolt (assume 1" diameter bolt)

$Ab = .25*\prod*D^2$

$Ab = .25*\prod*(1)^2$

$Ab = .7854\ in^2$

f'm = compressive strength of masonry

f'm = 1500psi

fy = yield strength of steel anchor bolt

fy = 84 ksi (group B bolts with treads excluded from the shear plane)

Apt = projected area for axial tension

$Apt = \prod*Lb^2$ eq. 1-4

Lb = bolt embedment length, min of 4 diameters,

Lb = 4" (assume 1" bolt)

$Apt = \prod*(4)^2$

$Apt = 50.27\ in^2$

$Bvnb = 4*22.83*(1500)^{.5} = 3537$ lb

$Bvnc = 1050*(1500*.7854)^{.25} = 6151$ lb

Bnvpry = 8*50.27*(1500).5 = 15562 lb

Bvns = 0.6*.7854*84000 = 39584.2 lb

Bvnb = 3537 lb controls

ΦBvnb = .8*3537 = 2829 lb

Φ = .8 (§3.1.4.4)